NASA CR 159570

DEVELOPMENT PROGRAM ON A COLD CATHODE ELECTRON GUN

(NASA-CR-159570) DEVELOPMENT PROGRAM ON A COLD CATHODE ELECTRON GUN Final Report (SRI International Corp., Menlo Park, Calif.) 82 p HC A05/MF A01 CSCL 09A G3/33

N81-19395

Unclas 18084

Final Report

May 1979

By: C. A. Spindt, Senior Research Engineer
Physical Electronics Group
Engineering Sciences Laboratory

Prepared for:

NASA-Lewis Research Center
21000 Brookpark Road
Cleveland, Ohio 44135

NASA Contract No. NAS 3-20096

SRI Project 5413

SRI International
333 Ravenswood Avenue
Menlo Park, California 94025
(415) 326-6200
Cable: SRI INTL MNP
TWX: 910-373-1246

SRI International

DEVELOPMENT PROGRAM ON A COLD CATHODE ELECTRON GUN

Final Report

May 1979

By: C. A. Spindt, Senior Research Engineer
Physical Electronics Group
Engineering Sciences Laboratory

Prepared for:

NASA-Lewis Research Center
21000 Brookpark Road
Cleveland, Ohio 44135

NASA Contract No. NAS 3-20096

SRI Project 5413

Approved:

Fred J. Kamphoefner, Director
Engineering Sciences Laboratory

Earle D. Jones, Executive Director
Advanced Development Division

CONTENTS

ILLUSTRATIONS

Illustrations---Continued

TABLES

I INTRODUCTION

This report summarizes the results of a feasibility demonstration program using the SRI-developed thin-film field-emission cathode (Spindt-type TFFEC) in a cold cathode electron gun structure suitable for high power microwave tube applications. The ultimate objective of this program was the production of a gun capable of 95 mA in a 0.26-mm diameter beam at 20 kV. The two major areas of effort were: (1) advancement of the cathode art to produce cathodes capable of 95 mA, and (2) the development of a gun structure to produce a 0.26-mm diameter 95-mA beam at 20 kV using the TFFEC. About 92 cathodes were tested; 81 worked, and 11 were taken to 95 mA or higher in a diode tube configuration. Several gun designs were investigated, and a prototype was fabricated and delivered to the National Aeronautics and Space Administration (NASA) for evaluation. NASA will perform high-current tests of the gun configuration using a beam tester designed for this purpose.

The Spindt-type TFFEC, which was the primary subject of the investigation described in this report, is based on the well-known field-emission effect and was conceived to exploit the advantages of that phenomenon while minimizing the difficulties associated with conventional field-emission structures, e.g., limited life and high voltage requirements. Field emission has been shown to follow the Fowler-Nordheim equation[1]*

$$J = \frac{A\ F^2}{t^2(y)\phi}\ \exp - \frac{Bv(y)\phi^{3/2}}{F} \qquad (1)$$

where J is the emission current density in A/cm^2, A and B are constants, F is the field at the tip, ϕ is the work function in eV, and v(y) and t(y) are slowly varying functions of y where

$$y = \frac{3.79 \times 10^{-4} F^{1/2}}{\phi} \qquad (2)$$

Both v(y) and t(y) are tabulated in the literature[2]. The field at the tip is

$$F = \beta V \text{ volts/cm} \qquad (3)$$

where V is the voltage applied to the diode structure and

$$\beta = f(r,R,\theta)\ cm^{-1} \qquad (4)$$

*References are listed at the end of this report

The relationship between f and the tip radius (r), the anode-to-tip spacing (R), and emitter cone half angle (θ) is complex[3] and difficult to determine accurately; for the purpose of our work we need only to note that as r, R, and θ become smaller, β increases. Thus, smaller cathode-anode structure reduces the voltage required for a given emission current.

The conventional field emitter, shown in Figure 1, consists of a short segment of fine wire (usually tungsten) etched electrolytically at one end to a sharp point (i.e., small r). The segment is mounted on a hairpin filament for support, and then is cleaned by passing current through the hairpin filament an heating the tip to incandescence. The point supplies cold electron emission when a positive voltage is applied to a ring or aperture anode spaced at a macroscopic distance ($R \leq 1.0$ cm) from the emitter tip. At the point surface, the electric field required for field emission is on the order of 10^7 V/cm; so despite the local field enhancement resulting from the sharpness of the tip, anode potentials of the order of kilovolts are usually required for field emission from a conventional emitter structure.

So we find that in conventional structures positive ions formed at the anode or between the anode and the sharply curved emitter are directed toward the tip by the curved field lines. These ions can roughen or sharpen the tip by sputtering. The sputtering efficiency is determined by a rate of ion formation, which is directly related to the local vacuum pressure and emission current drawn, and by the ion energies, which depend on the applied voltages. Tip sharpening by ion sputtering during operation increases the local field (for the same applied voltages) and thus progressively increases the emission current and the sputtering rate until resistive heating of the tip leads to its destruction. This effect places a severe limit on useful lifetimes for conventional emitters; but Brodie[4] has shown that the sputtering effect can be greatly reduced if one can lower the emission voltage below 150 V, and that reduction of the applied voltage to $\sim$ 50 V may effectively eliminate the sputtering.

From an examination of the conventional structure we see that operation of dense arrays of parallel tips entails difficulties of fabrication and that neighboring tips have a mutual shielding effect. Thus, large emitter-array areas that produce high current densities have not yet been achieved by these means.

The field emission cathode shown in Figure 2 was developed at SRI. It consists of a conductor/insulator/conductor sandwich of dielectric thickness about 1-1/2 μm, with holes about 1.5 μm to 2 μm in diameter in the top conductor (metal gate film), undercut cavities in the dielectric layer, and metal cones within the cavities.

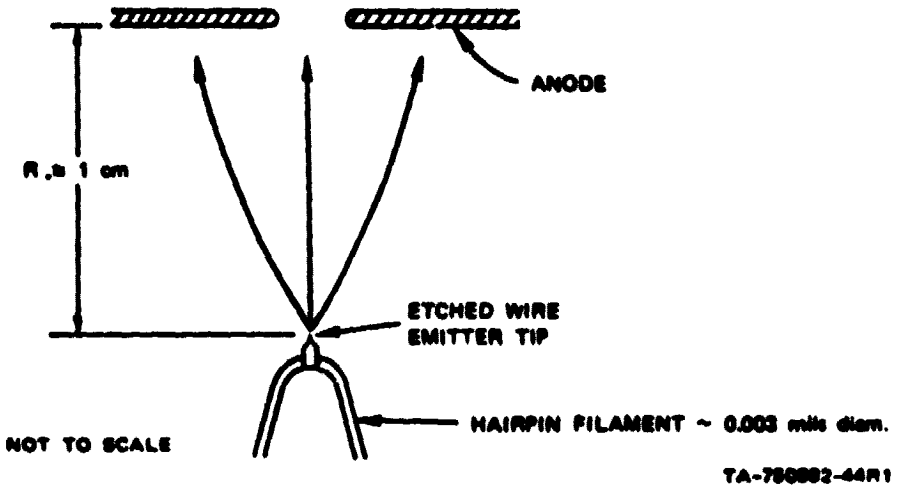

FIGURE 1 CONVENTIONAL FIELD EMITTER AND ANODE

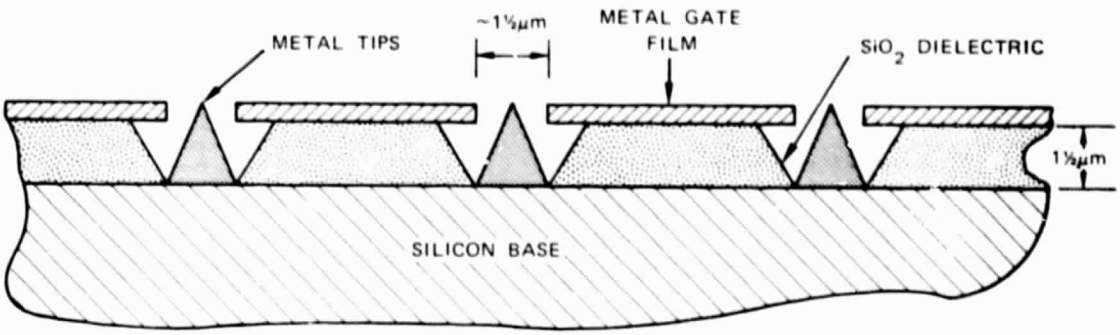

(a) SCHEMATIC OF A THIN-FILM EMISSION CATHODE ARRAY

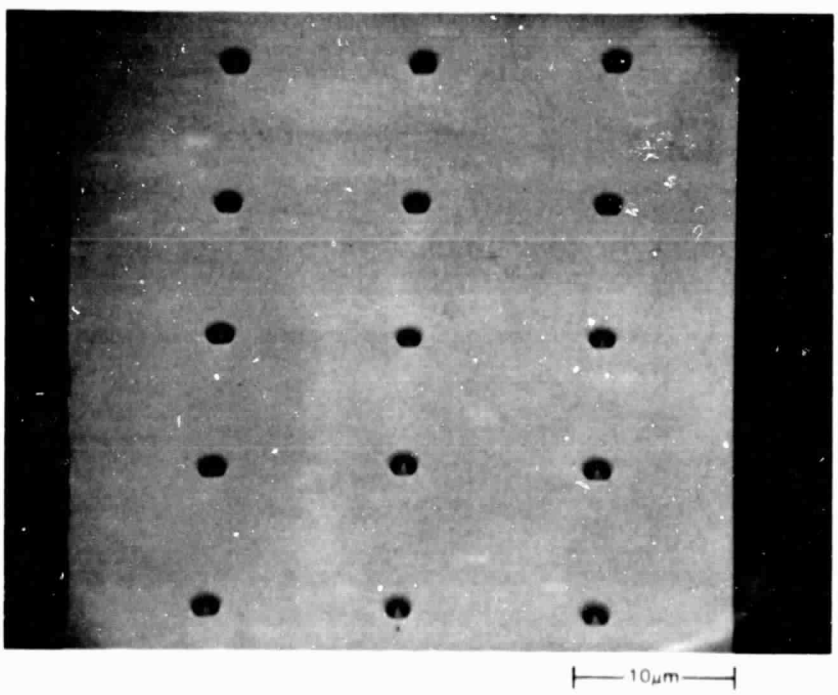

(b) SCANNING ELECTRON MICROGRAPH OF A CATHODE ARRAY

FIGURE 2 THE SPINDT-TYPE THIN-FILM FIELD-EMISSION CATHODE

Field emission is obtained from the tips of the cones when the tips are driven negative with respect to the gate film. The field enhancement of the tip (small r) and the close spacing between the rim of the hole in the gate film and the tip (small R) require potentials of only 100 V to 200 V across the sandwich for large field-emission currents. In addition, dense arrays of tips can be operated without influencing one another; the gate film surrounds each cone and prevents reduction of the electric field at the tips caused by tip interaction.

This configuration reduces the problem of ion bombardment because the tips are well shielded electrostatically by the gate film; that is, the equipotentials contoured about the tip are essentially confined within the cavity and the equipotentials between the gate film and other external acceleration electrodes are uniformly spaced and plane parallel. Thus, unlike the etched-wire configuration case most ions formed between the gate film and an external acceleration electrode are directed toward the gate film rather than the tip. Also, the volume of ionization between the gate film and the tip is very small; any ions formed within this region will have low energies and will be unlikely to cause significant sputtering damage by striking the tip.

II EXPERIMENTAL RESULTS

A. Purpose of the Experimental Program

The experimental and developmental program was directed toward production of an electron beam of 95 mA in a 0.26-mm diameter beam at 12 kV. The realization of these goals required development work in the following areas:

- Cathode production
- Anode or collector development for high current tests
- Analysis and minimization of high-current cathode-failure mechanisms
- Development of cathode driving circuits
- Electron optics studies using rubber membrane and computer models
- Design and fabrication of an electron optics bench
- Studies of electron-gun structures using the electron optics bench
- Energy-spread measurements
- Development of a precision cathode mount
- Delivery of a prototype electron gun with an operating cold cathode.

B. Fabrication Technology

Cathodes fabricated and tested on this program all consist of a 5000-tip array with the tips on 12.5-μm centers. The array covers an area 1 mm in diameter on a silicon chip that is nominally 2.5-mm square. This cathode type has been designated "type 20" in the SRI cathode series. The fabrication process was essentially similar to that developed on the preceding program (NASA Contract NAS3-18903). Process yield improvements resulted from improved operator skills (through increased familiarity with the process) and from experiments with the process variables to determine optimum conditions concerning film adhesion, hole/cone geometry, and etch rates.

The basic cathode fabrication process for these studies was as follows:

(1) Two-inch diameter silicon wafers were oxidized to a depth of 1.5 μm by standard oxidation techniques developed in the semiconductor industry.

(2) The wafers were cut into 1/2-inch squares by scribing and breaking, or sawing with a dicing saw.

(3) Molybdenum electrodes were deposited onto the squares by electron beam evaporation. The electrodes were about 4500 Å thick and were 0.070-inch square, spaced on 0.100-inch centers. Thus, there were 25 electrodes on each 1/2-inch substrate.

(4) Aluminum was then deposited over the substrate surface between the molybdenum electrodes to protect the silicon dioxide during subsequent processing, and to establish electrical contact between all the electrodes and the substrate.

(5) An electron-sensitive resist, poly(methyl-methacrylate) or PMM, was applied to the substrates and patterns of ~ 1-μm diameter holes exposed with the SRI screen lens system. The patterns were 0.040 inch (~ 1 mm) in diameter and contained about 5000 holes on 0.0005-inch centers.

(6) Holes were etched in the molybdenum electrodes where the molybdenum had been exposed by developing the hole pattern in the PMM.

(7) The PMM was stripped from the substrate and the silicon dioxide was etched down to the silicon base where it had been exposed by the holes in the molybdenum film.

(8) The substrate was then mounted on a vacuum deposition station; the substrate was rotated about an axis perpendicular to its surface as a pre-closing/parting layer was deposited at a grazing angle.

(9) The substrate was broken into twenty-five 0.100 X 0.100-cathode chips for mounting in the cone deposition apparatus, and molybdenum cones were deposited into the partially closed holes.

(10) The parting layer was then dissolved releasing the top molybdenum film deposited during cone formation and leaving the completed cathode chips with ~ 5000 emitter tips in a 1-mm diameter area.

(11) The chips were mounted in high-temperature ceramic holders for electrical tests.

1. Film Adhesion and Etch Factors

Several changes were made during the program in details of the process steps to improve film purity, film adhesion, and the geometry of the etched holes. The scope of the program did not permit an extensive and systematic investigation of these parameters, but the chosen empirical approach resulted in an improved structure and demonstrated dramatic variations in the results with variation in process parameters.

The molybdenum gate-film deposition process was the most interesting. Midway through the program SRI obtained an ion-pumped deposition system suitable for gate film and cone deposition. Background gases and system cleanliness can influence the nature of deposited films and a well-maintained 10^{-9} torr ion pumped vacuum is cleaner than our 10^{-6} torr oil-pumped system (used in routine film deposition service for over 10 years). We felt that a field emitter cathode tip formed of materials deposited in a clean environment would be better behaved than would one of less certain composition. From the first, these assumptions seemed to be well founded; we obtained superior etching characteristics with substrates whose gate films were deposited in the ultravacuum system--specifically the silicon dioxide etch factor (ℓ/d) as shown in Figure 3.

Samples whose molybdenum gate films were deposited in the oil pumped system after sputter cleaning of the substrate with an oxygen/argon plasma produced etch factors as large as 1.8 (ℓ_2/d in Figure 3). This severe undercutting of the gate film led to cracking and breaking of the unsupported portion during subsequent processing. It also imposed a basic limit to the packing density that could be achieved with a given oxide thickness.

Gate films were deposited in the ultra-high vacuum (UHV) system using the same electron beam evaporator that was used in the high-vacuum depositions. The predeposition in situ substrate cleaning consisted of a 600°C bake rather than the plasma/sputter cleaning used in the high vacuum system. This heat cleaning was substituted for the plasma/sputter cleaning because of the reduced pumping capacity of the ion pumped system. The resulting gate films were smooth and bright, and produced an etch factor in the SiO_2 etch of 1 (wall slope of 45°), a significant improvement over the etch factor of 1.8 obtained with gate films deposited in the high vacuum station using plasma/sputter cleaning.

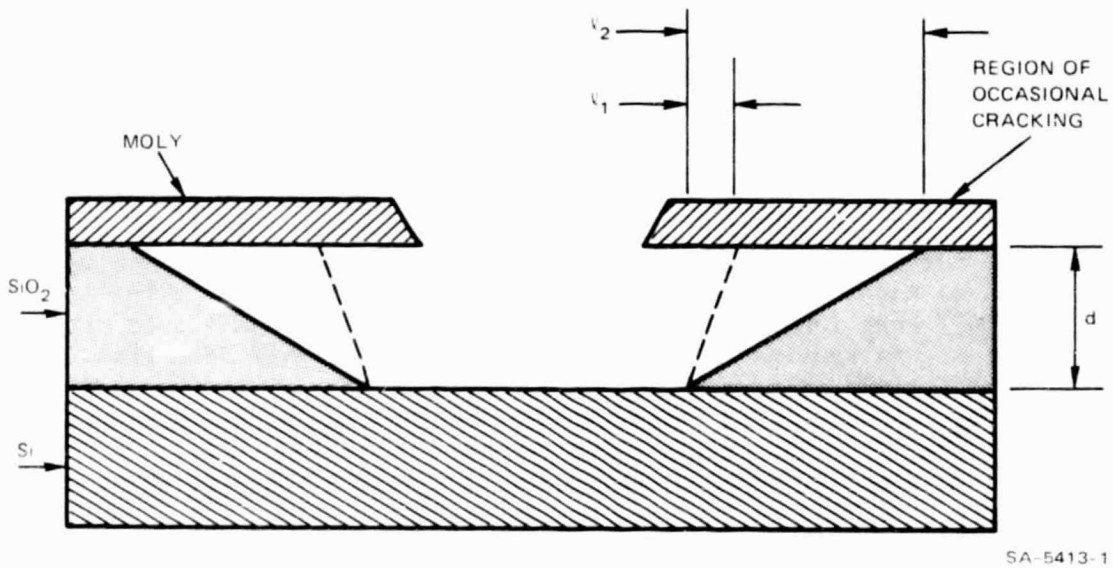

FIGURE 3 ETCH FACTORS (ℓ/d) AND THE AREA IN WHICH CRACKING OF THE MOLYBDENUM GATE FILM CAN OCCUR IF ℓ/d BECOMES LARGE

This improvement was attributed initially to better adhesion between the gate film and SiO_2 resulting from the combination of a cleaner vacuum environment and the heat cleaning used prior to deposition. Therefore, it was rather surprising to discover that the gate film broke up and lifted away from the SiO_2 during subsequent processing. These results are contradictory and not yet understood, but it is known that heating samples improves bonding, and that some oxygen can improve the adhesion of active metals to substrates. So gate films were deposited in the high-vacuum system (10^{-6} torr) with the 600°C substrate bake, based on the assumption that the 600°C substrate bake in ultra-high vacuum was helpful and that the 10^{-9} torr environment resulted in a deficiency of oxygen at the interface between the molybdenum gate film and the SiO_2. The resulting films produced an etch factor of 0.7 (35° wall slope) in the SiO_2, and they did not lift from the substrate during subsequent processing as did the films deposited in UHV.

This very much reduced etch factor also makes possible higher-packing-density cathodes. As can be seen from the micrographs in Figure 4, it would be impossible to increase the packing density with the 1.8 etch factor shown in 4(a), but Figure 4(b) shows an etch factor of 0.7 obtained with the improved processing. It is clear from Figure 4(b) that it is reasonable to try to increase the packing density of this structure by decreasing cavity size through the use of thinner oxide and a smaller diameter hole in the gate film.

Figure 4(a) shows a completed cathode with a portion of the moly gate film broken away to expose the underlying structure. In Figure 4(b), all of the moly gate film and cones have been chemically etched away to show the SiO_2 etch factor; the bond between the gate film and the SiO_2 was too strong to be broken as we did with the cathode shown in Figure 4(a).

2. Decreasing Hole Diameter for Increased Packing Density

It will not be possible to further reduce the size of the cathode hole/cone structure beyond some practicable limit. The limit may be associated with oxide thickness and dielectric breakdown; a practicable minimum in the closure/parting film thickness below which parting is unreliable, limits in the minimum hole diameter that can be reliably exposed in our electron sensitive resist (taking into account the backscattering that occurs as the beam impacts the substrate), or some other factor. These limiting factors must be investigated and each step of the process optimized to achieve the practicable limit. This has been set aside for future programs. For now, it is worthy of note that structures significantly smaller than we are now fabricating are possible, as shown by results obtained with a cathode that had a faulty resist layer and developed several "pinholes" (many of which were smaller than the holes we normally fabricate in the moly gate film). Figure 5 shows an electron micrograph of a portion of this cathode with one hole 2 μm in diameter containing a large

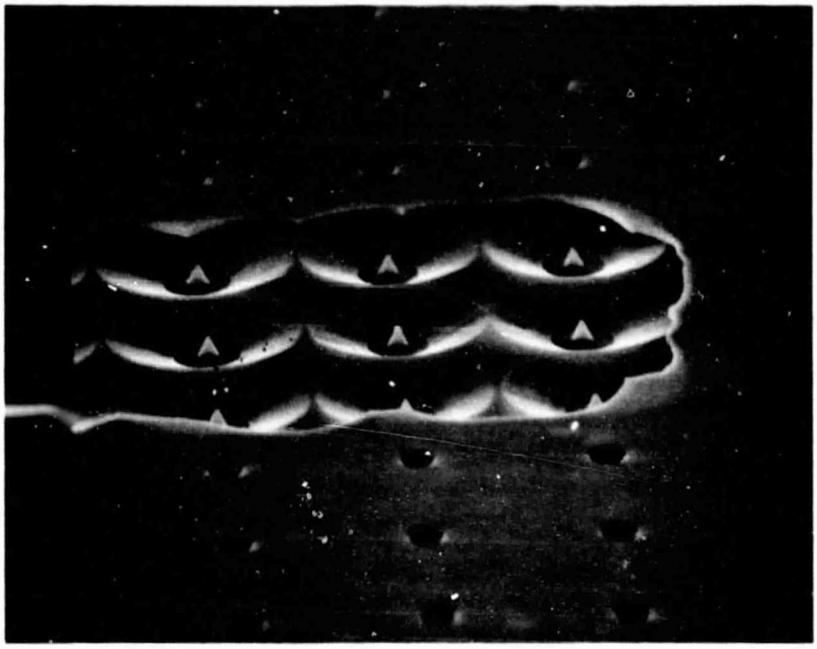

(a) CATHODE WITH A PORTION OF THE GATE FILM BROKEN AWAY TO SHOW A SiO_2 ETCH FACTOR OF 1.8

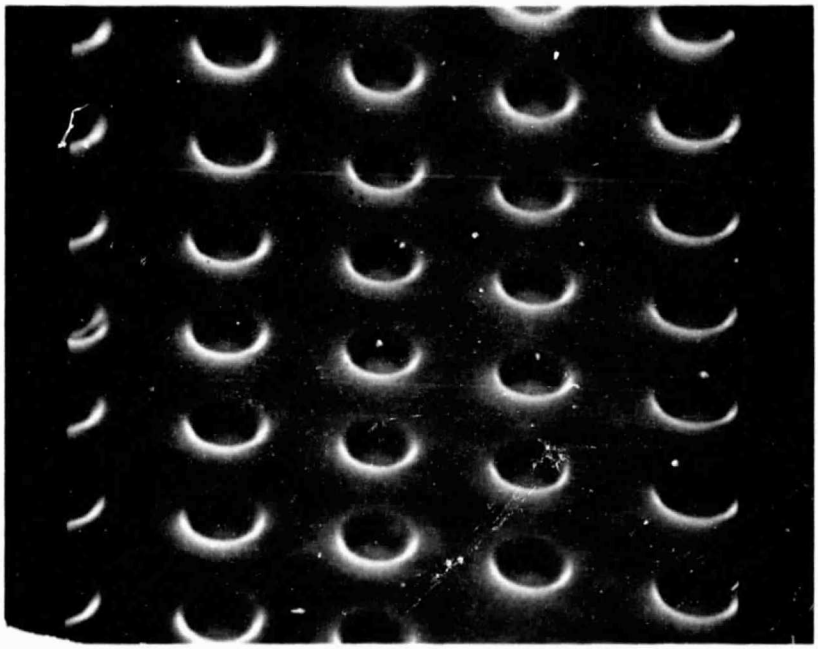

(b) CATHODE WITH ALL MOLYBDENUM ETCHED AWAY SHOWING A SiO_2 ETCH FACTOR OF 0.7

FIGURE 4 VARIATIONS IN SiO_2 ETCH FACTORS

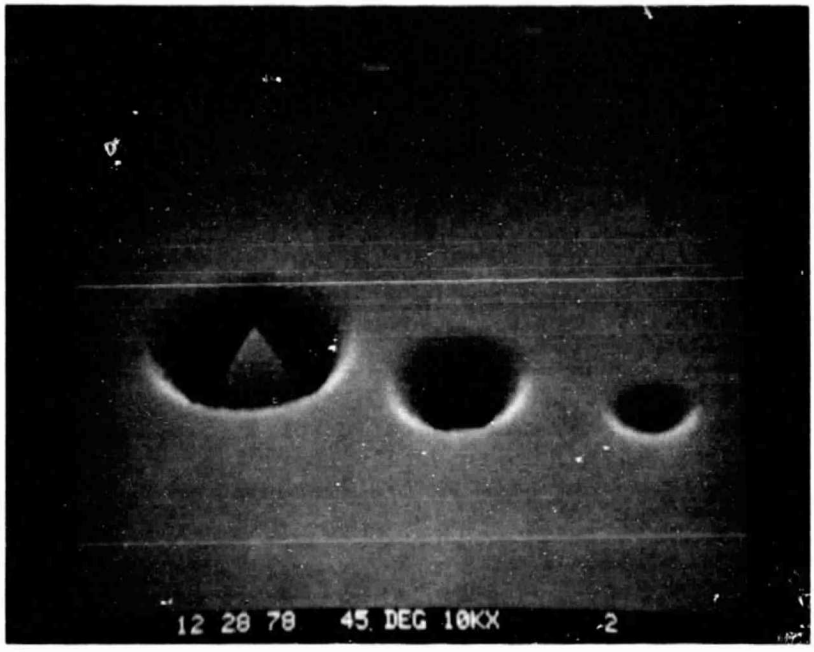

FIGURE 5 SCANNING ELECTRON MICROGRAPH OF A 2-μm DIAMETER CATHODE AND A 0.85-μm DIAMETER CATHODE SPACED 3-μm CENTER-TO-CENTER

cone and a nearby hole with a 0.85 μm diameter hole and proportionally smaller, certainly adequate, cone. The cones are approximately 3 μm between centers. Making 0.85 μm holes in a controlled process will require some work with our screen lens electron beam exposure system, but it should be possible.

C. High Current Operation

A cathode has been tested at currents of up to 160 mA, 20 A/cm^2 from the 1-mm diameter area occupied by the 5000-tip array. Ten have been tested above 95 mA or 12 A/cm^2 without suffering significant tip failure counts; four cathodes were operated at over 95 mA with fewer than 5 (0.1%) tip failures. In addition, two 100-tip arrays have been operating on life test at 2 mA for 33,000 hours (3 years, 9 months) with no change in operating parameters since emission was established. These life tests are discussed in detail in Section E. The life test results are significant with regard to high-current operation because when operating at an emission level of 2 mA, the 100 tip array is working at an average tip loading of 20 μA per tip. Thus it appears that the difficulties encountered in achieving 100 mA routinely with the 5000-tip array are aassociated more with the total current level and its impact on the tube components than with a basic cathode limitation. For example it was necessary to use pulsed operation to prevent overheating the collector or anode, but a high frequency pulse generator used for this purpose caused arcing damage to the cathode. Attempts to use water-cooled copper anodes led to large numbers of tip failures by local arcing. High-current operation required high fields between the cathode and the collector to overcome space charge effects, but increasing the voltage on the collector led to heating and breakdown problems. These and other effects are discussed in more detail below.

1. Space Charge Effects

Observation and analysis of the behavior of gate film current when operating the cathode at high emission levels give a clear indication of space charge effects in the beam. Figure 6 shows the circuit used and the various observed sources of gate current. Typical operation has been with the gate grounded through one channel of a dual-trace oscilloscope, the tips driven negatively by a 60-Hz half wave rectified sine wave, and the collector biased positively about 1 kV to accelerate the electrons away from the cathode and prevent losses due to secondary emission from the collector. Normal emission from the tips to the collector is shown in Figure 6 by the trajectory labeled (1). Numbers 2, 3, 4 and 5 show various sources of gate current. Figure 7 shows oscillographs illustrating different gate current conditions; Figure 7(a) shows 45 mA of emission to the collector with about 35 μA in the gate film circuit. The V-I trace for the gate circuit indicates cathode capacitance by the hysteresis or capacitive loop that the trace follows (#5 in Figure 6), some cathode leakage (#4 in Figure 6) by the slight droop in the trace as voltage increases, and condition 2 in Figure 6 by the sudden and steep drop in the trace near peak voltage. This steep break is surely intercepted emission current,

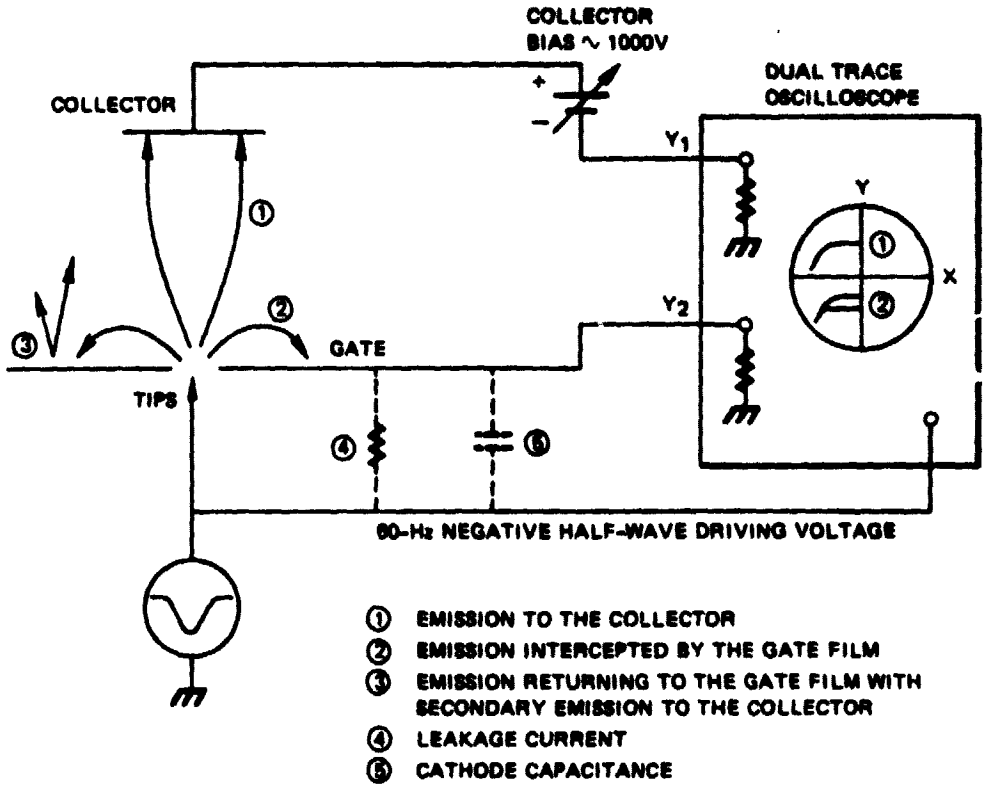

FIGURE 6 SCHEMATIC OF THE TEST CIRCUIT SHOWING GATE CURRENT SOURCES

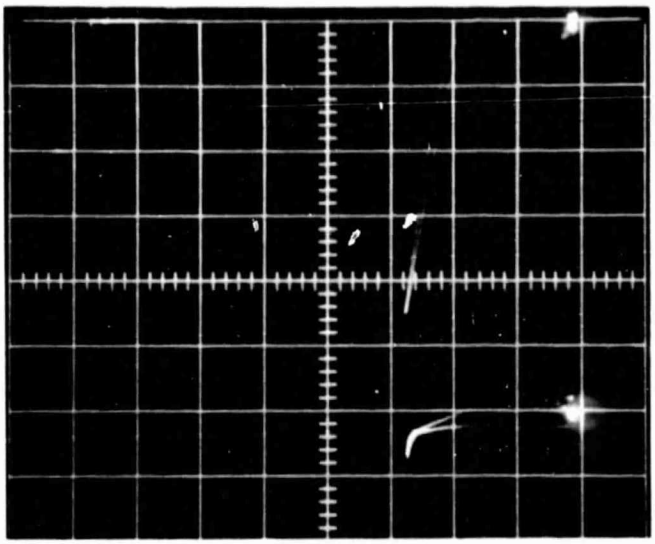

TOP TRACE:
Y = 10ma/cm
X = 50V/cm
BOTTOM TRACE:
Y = 50μa/cm
X = 50V/cm

(a) INTERCEPTED EMISSION AND SOME LEAKAGE

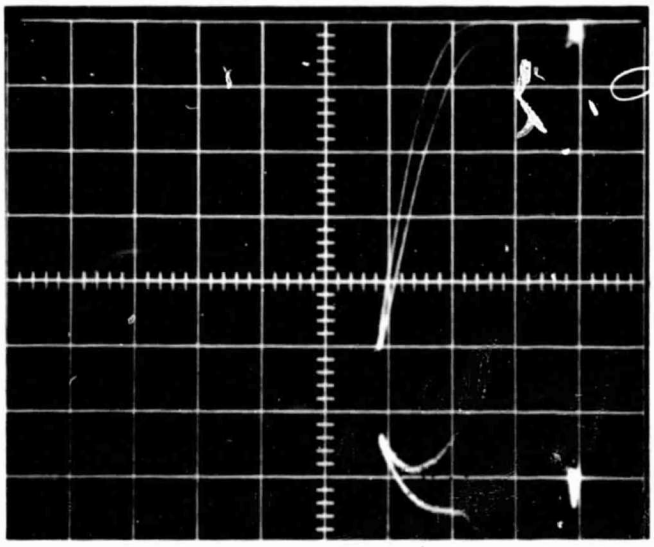

TOP TRACE:
Y = 10ma/cm
X = 50V/cm
BOTTOM TRACE:
Y = 10μa/cm
X = 50V/cm

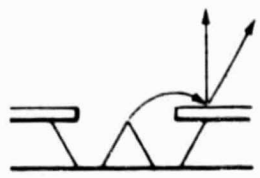

(b) INTERCEPTED EMISSION WITH SECONDARY EMISSION RATIO GREATER THAN 1

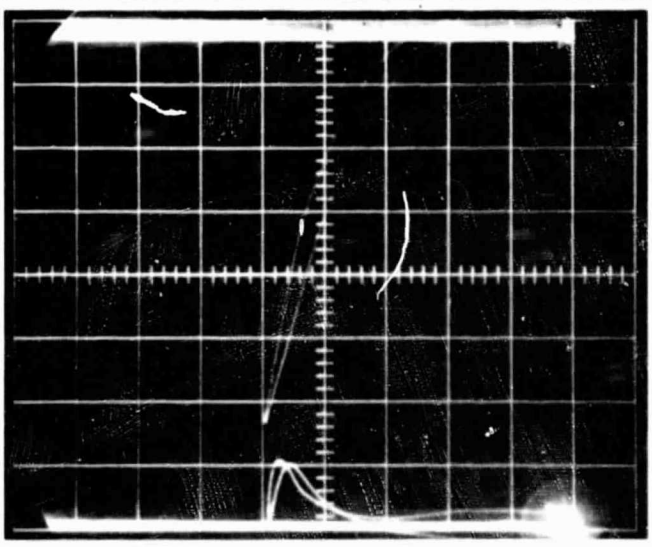

TOP TRACE
Y = 25ma/cm
X = 50V/cm
BOTTOM TRACE
Y = 50μa/cm
X = 50V/cm

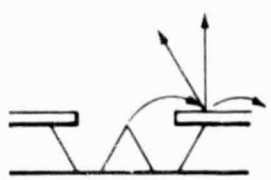

(c) INTERCEPTED EMISSION WITH SECONDARY EMISSION GREATER THAN 1, BUT WITH SPACE CHARGE PREVENTING ESCAPE OF SECONDARIES AT PEAK EMISSION

FIGURE 7 DIFFERENT GATE-CURRENT MODES

and is very likely due to space charge effects; we found that increasing the voltage on the collector reduced the amount of current going to the gate.

Figure 6(b) shows reverse current flow in the gate circuit, but again increasing the collector voltage caused the gate current to be reduced in value indicating that space charge effects were causing electrons from the beam to return to the gate film as shown by condition 3 in Figure 6. In this case, the impact was apparently at a location on the gate film which prevented the escape of secondaries to the collector. Under these conditions, a secondary emission ratio greater than 1 would give the impression that positive ions were going from the collector to the gate, or that the gate was field emitting to the collector.

The conclusion that it is in fact secondary emission to the collector is supported by Figure 7(c). The emission to the collector is very high (about 160 mA) and the current to the gate is seen to go positive initially and then to decrease so that at the peak voltage there was a net zero current flow in the gate circuit. When the collector voltage was again decreased from 1 kV, the magnitude of the current to the gate film increased slightly; increasing the collector voltage to 1200 V decreased the magnitude of the gate current.

It appears from these results to be necessary to maintain fairly high electric fields at the cathode surface to prevent space charge effects in the beam from causing bombardment of the gate film. Care is required because fields are increased by raising voltage and decreasing spacing; both can cause difficulties with the experiment. Higher voltage increases collector heating and outgassing which can lead to breakdown,; closer spacing leads to higher current density at the collector and less favorable local pumpout conditions, which can also lead to breakdown.

2. Collector Heating

High peak-power density caused difficulty in the high current experiments. We found that the collector was heated to incandescence ($\sim$ 900°C) in a matter of moments when operated at 15 mA peak collector current with a negative half sine wave 60 Hz tip driving voltage, +300 V on the collector, and the gate film at ground. This problem was eliminated by devising a low duty cycle pulsing circuit to drive the cathode.

The low duty cycle circuit worked well, but disturbing failures of the gate film occurred when the cathode was operated in a pulse mode to minimize collector heating. These failures were "chain lightning" arcs across the surface of the gate film as shown in Figure 8. It was noted that this failure was not necessarily associated with high emission-current levels; they occurred only when a cathode was driven with the pulse circuit that had been designed for operating the cathodes at a low duty cycle during high emission current tests. The low duty cycle pulse circuit

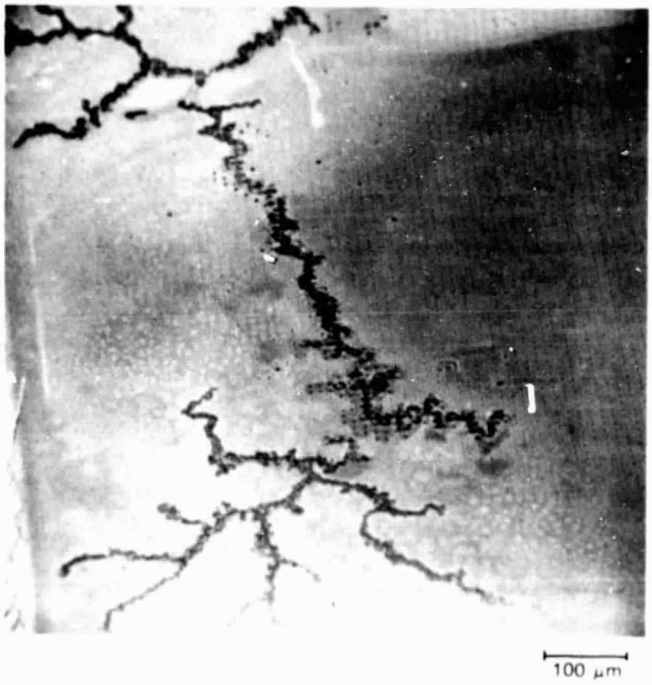

FIGURE 8 MICROGRAPH OF ARC DAMAGE ON THE GATE FILM OF A TFEC AFTER HIGH-FREQUENCY PULSE OPERATION

consisted of a dc power supply and a gating circuit to turn a dc voltage to the cathode on and off very rapidly with a low repetition rate. Figure 9 shows the voltage pulse applied to the base and the resultant emission current pulse applied to the collector. It appears that the fast rise time of the pulse compared with 60-Hz operation resulted in charging currents in the gate film high enough to produce local outgassing and breakdown shown in Figure 8.

Clearly, it was necessary to overcome these problems (space charge, collector overheating, and excessive charging currents in the gate film) to achieve emission currents in the 100-mA range.

Breakdown caused by high charging currents in the gate film was the first difficulty to be eliminated. Early work with 100-tip arrays demonstrated that the cathode was capable of being driven at peak voltages in the 400-V range when using a 60-Hz sine wave. Thus, a gating circuit was devised to gate the output from our 60 Hz half wave rectified cathode supply and allow only a predetermined fraction of the 60 pulses per second through to the cathode. The gating circuit can be adjusted to reduce the duty cycle to 10%, 2%, 1%, 0.5%, 0.2%, and 0.01% of the normal 60 pulses per second. Figures 10 and 11 show the gating circuit used. There have been no "chain lightnening" cathode gate-film failures when operating the cathodes with this circuit, but there were several failures in the form of a high-energy localized arc as shown in Figure 12.

These failures were caused by high output capacitance in the gating circuit design. The laboratory in which the experiment was being conducted has a great deal of electrical noise, and a capacitor had been added to the output of the gating circuit to minimize electrical spikes which could cause high frequency pulses and the "chain lightning" arc experienced with the square wave pulse. The capacitor worked well for this purpose. But if a single tip failed to a short circuit when the capacitor was charged to peak voltage, the energy stored in the capacitor was dumped into the gate film through the short and the sandwich structure was literally blown apart. This gross damage usually resulted in a permanent short between the cathode base and gate film.

When the cause of the problem was diagnosed and the capacitor replaced by a power line filter and improved shielding, this failure became uncommon.

These changes resulted in improved performance, nevertheless the cathodes suffered a disturbing number of individual tip failures at currents well below that expected on an individual-tip-loading basis. As measurements with 100-tip arrays yielded currents that averaged 20 μA per tip with ease, the 5000-tip-array cathode could be expected to produce a total of 100 mA or 20 μA per tip without undue difficulty. But this was not the case: individual tip failures occurred at loadings of about 5 μA per tip in

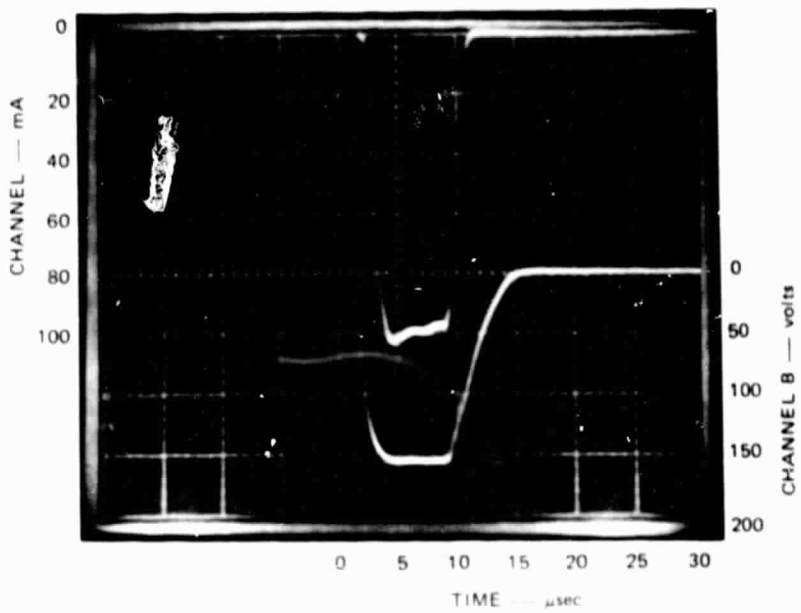

FIGURE 9 PULSE OPERATION OF A 5000-TIP TFFEC, APPLIED VOLTAGE 150 VOLTS, EMISSION CURRENT 100 mA

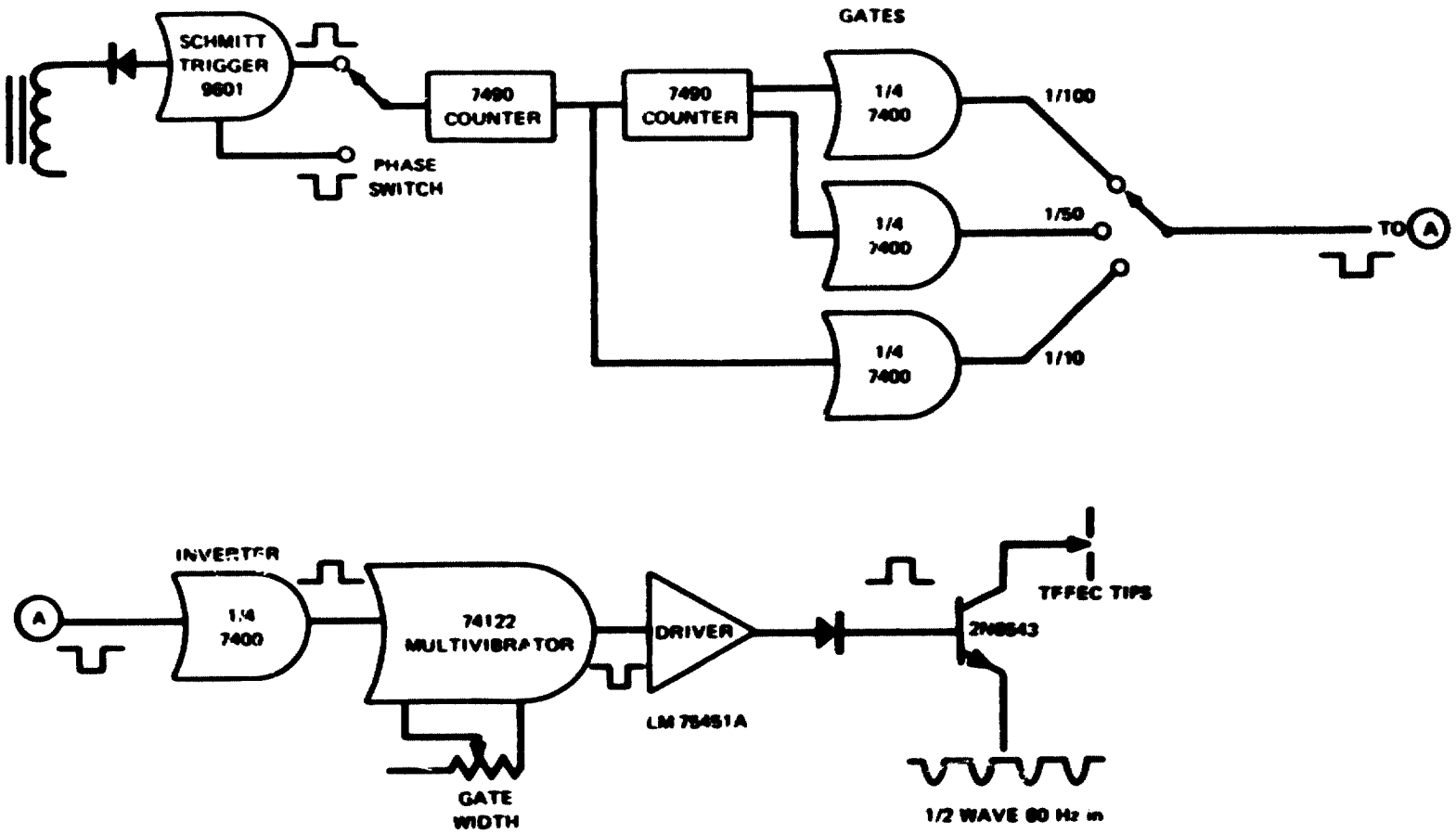

FIGURE 10 BLOCK DIAGRAM OF CIRCUIT FOR HIGH CURRENT EMISSION TESTS

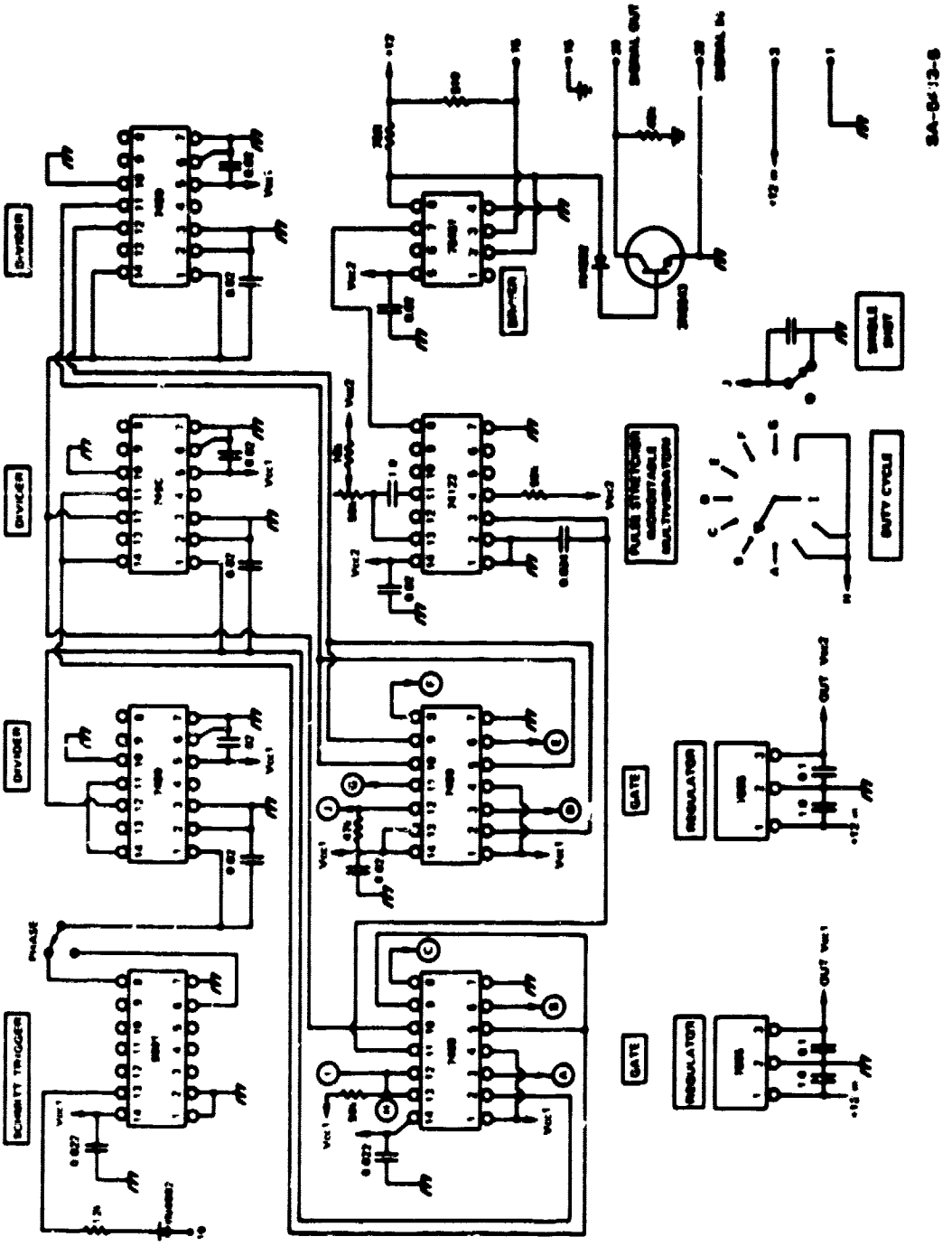

FIGURE 11 PULSE CIRCUIT FOR DRIVING CATHODES

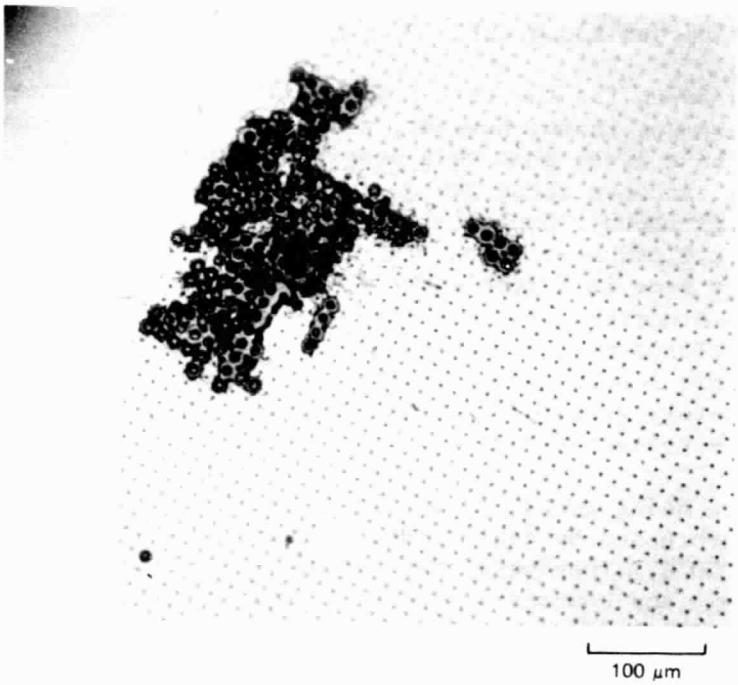

FIGURE 12 MICROGRAPH OF A LOCALIZED HIGH ENERGY ARC ON THE TFFEC SURFACE

large numbers of the 5000-tip cathodes (see Figure 13(a)). This result suggested that the higher total currents produced by the 5000 tip array cathode were causing heating of the collector and bursts of gas that caused arcs in the cathode structure even with the reduced duty-cycle operation.

In an attempt to reduce collector heating and outgassing, a water-cooled OFHC copper collector was fabricated as shown schematically in Figure 14. The collector was cleaned by baking in ultra high vacuum to 450°C while the end was bombarded with electrons from a hot tungsten wire filament. The cathodes were then installed and the system again baked to 450°C before the cathodes were turned on. The results were surprisingly poor, and the cathodes all failed to reach current loadings over about 1 μA per tip. Figure 13(b) shows the large numbers of tips that were typically found to have failed after a trial using the copper collectors: as many as 2500, or 50% of the total tips, were destroyed on some cathodes. Remarkably, some of these cathodes were still operating even after about 50% of the tips had blown out.

The reasons for the very poor results with the water-cooled copper collectors are not known; however, a simple collector arrangement reduced the problem to a level that made possible achievement of 100-mA emission with several cathodes using the gating circuit. The successful collector arrangement is shown schematically in Figure 15. It consists of a well-outgassed stainless steel tube 3/8" in diameter and about 1 inch long. The tubes are bent in a gentle curve, so that no direct path through exists for the electrons, but gas molecules can escape from either end. When the electrons from a cathode are directed into one end of the tube as shown, their landing area is spread over most of the inside wall of the tube, thereby greatly reducing the power density caused by electron impact on the collector surface.

Before being installed in the cathode test structure the collector tubes were processed by degreasing, hydrogen firing at 1000°C and vacuum baking at 1000°C. They were then pumped to about 10^{-9} torr in the ultra vacuum system and bombarded with electrons from a tungsten filament cathode at 500 V and 20 mA dc: the tubes were seen to glow at about 900°C during this bombardment. After 30 minutes under these conditions the filament and voltage were turned off and the tube allowed to cool. At the end of cool down the pressure was noted to be $\sim 2 \times 10^{-10}$ torr. The filament was then turned on again and a pressure burst of $\sim 6 \times 10^{-10}$ torr noted for a few moments. After this burst had settled, the voltage was applied to the tube and another pressure burst of about 4×10^{-10} torr was noted for about 10 seconds. The presssure was then stable at about 2×10^{-10} torr as the tube heated to ~ 900°C. After cool-down the chamber was opened to dry nitrogen and the tungsten filaments replaced with the field-emission cathodes. The system was then pumped down again and baked at 400°C for 48 hours. The cathodes were then brought up to 10 mA of emission slowly using the 60 Hz driving voltage at 100% duty cycle, 20 mA at 10% duty cycle and 100 mA at 1% duty cycle. The gating circuit shown in Figure 10 and described earlier was used to control the duty cycle. The results obtained are shown in Table I. The data in the table clearly show that cathode performance was significantly improved by using the stainless-steel tube collectors.

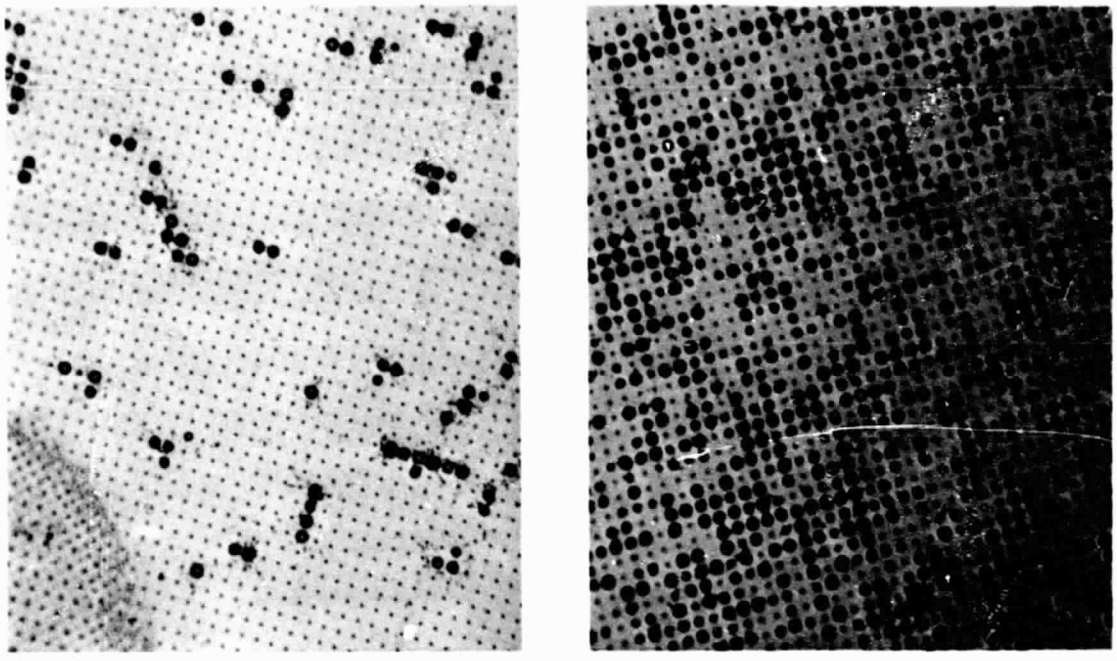

(a) 20mA

(b) 5mA

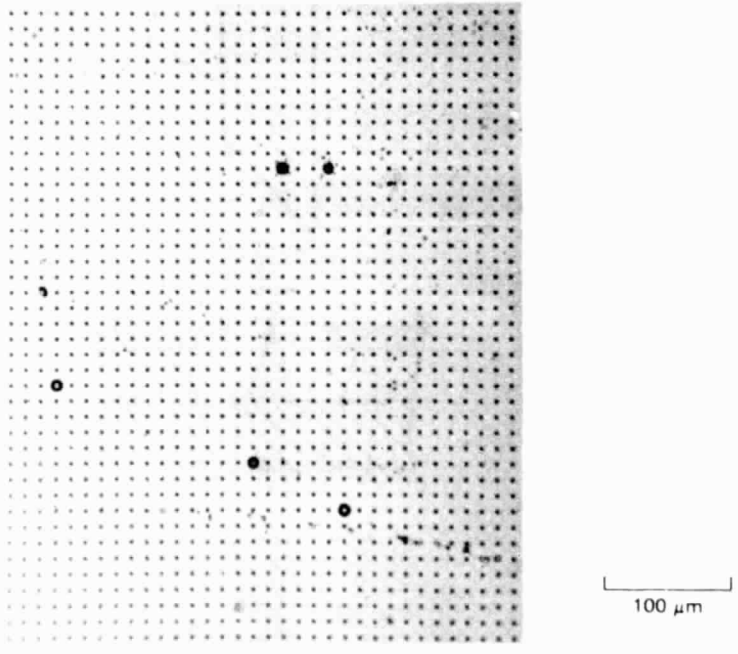

(c) 100mA

FIGURE 13 MICROGRAPHS OF INDIVIDUAL TIP FAILURES CAUSED BY LOCALIZED FAULTS AND HIGH-PRESSURE BURSTS

(a) Original molybdenum collector; (b) Water-cooled OFHC copper collector; and (c) Stainless-steel tube collector.

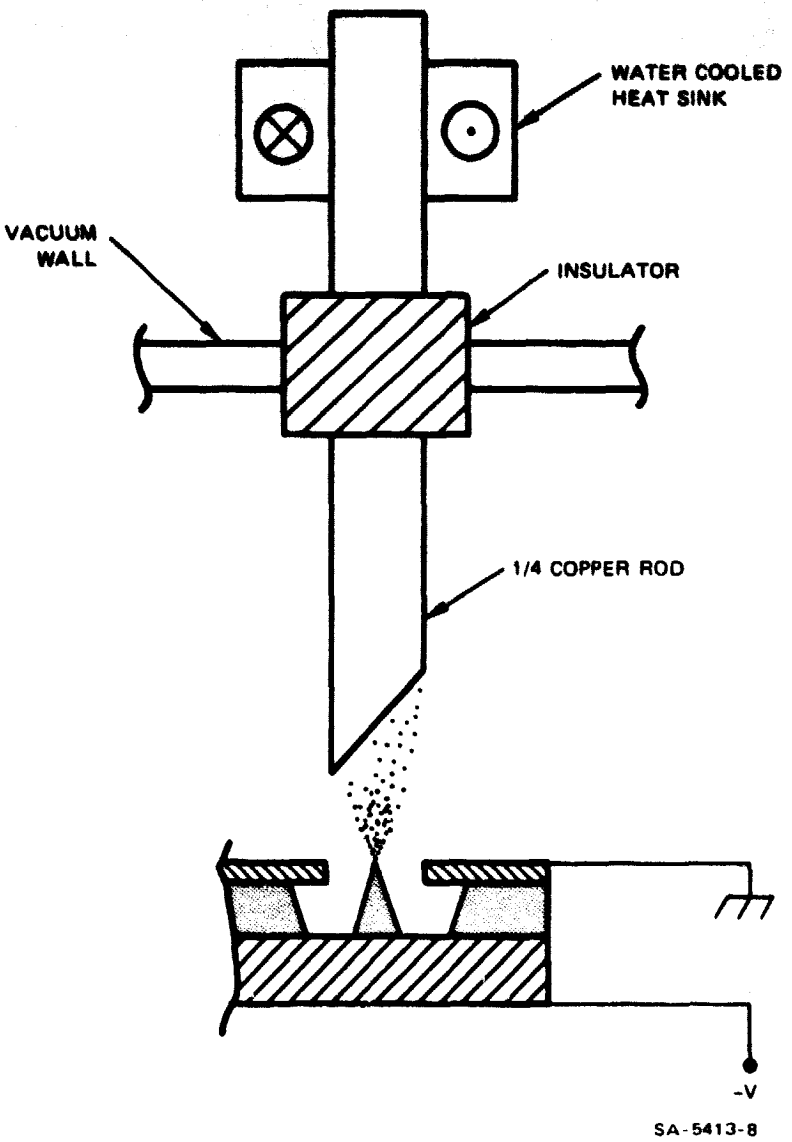

FIGURE 14 WATER-COOLED COPPER ROD COLLECTOR

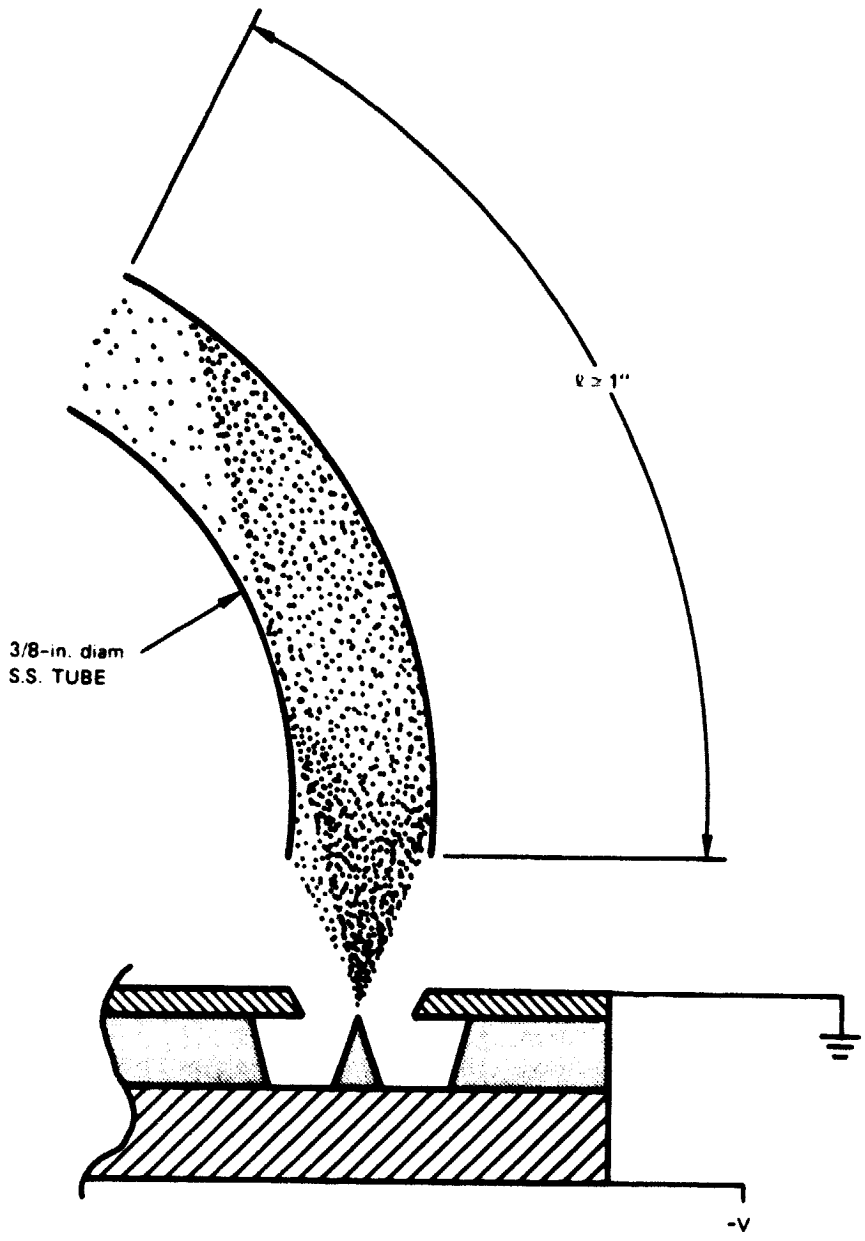

FIGURE 15 SCHEMATIC OF TUBE COLLECTOR PRINCIPLE FOR REDUCING CURRENT DENSITY AT THE COLLECTOR SURFACE

Table I

HIGH CURRENT TESTS

Test Set	Cathode Number	Maximum V/I	Duty Cycle	Anode Type	Tips Blown	Arcs	Remarks
1	20-9-1-B	180/10mA	100%	Moly	27	0	Shorted
1	20-9-1-C	205/10mA	10%	Moly	100	1	Shorted
1	20-9-1-F	280/20mA	1%	Moly	100	2	Shorted
1	20-9-1-G	175/5mA	100%	Moly	~1000	0	Shorted
1	20-9-1-H	300/20mA	10%	Moly	~300	1	Shorted
1	20-9-1-I	215/25mA	10%	Moly	17	1	Shorted
2	20-9-2-W	210/0.5mA	10%	S.S. Tube	0	2	Shorted
2	20-9-2-P	330/25mA	1%	S.S. Tube	0	2	Shorted
2	20-9-2-R	330/15mA	1%	S.S. Tube	30	1	Shorted
2	20-9-2-M	200/50mA	1%	S.S. Tube	1	0	OK
2	20-9-1-J	225/25mA	2%	S.S. Tube	0	1	Shorted
3	20-9-2-B	120/0.4mA	100%	Copper	~500	1	Shorted
3	20-9-2-I	185/7mA	100%	Copper	~300	1	Shorted
3	20-13-3-R	270/4mA	100%	Copper	2500	0	Shorted
3	20-13-3-T	190/4mA	100%	Copper	~300	0	Short
4	20-13-2-F	195/11mA	100%	Copper	~1000	0	Short
4	20-13-3-J	275/4mA	100%	Copper	~1000	0	Short
4	20-16-1-I	275/4mA	100%	Copper	1000	0	Shorted
4	20-16-1-K	155/3mA	100%	Copper	~3000	0	Shorted
5	20-14-1-R	270/6mA	100%	Copper	~1000	0	Working
5	20-14-3-M	150/5mA	100%	Copper	~2500	0	Working
5	20-14-3-N	215/7mA	100%	Copper	~2500	0	Working
6	20-9-2-Q	255/40mA	1%	S.S. Tube	115	0	Shorted
6	20-16-1-R	223/95mA	1%	S.S. Tube	181	0	Working
6	20-6-3-C	120/10mA	100%	S.S. Tube	15	0	Shorted
6	20-6-1-I	185/100mA	1%	S.S. Tube	5	0	Working
7	20-9-1-M	190/100mA	1%	S.S. Tube	3	0	Working
7	20-9-1-N	240/100mA	1%	S.S. Tube	108	0	Working
7	20-6-2-O	210/35mA	1%	S.S. Tube	49	0	Shorted
7	20-6-2-K	250/160mA	1%	S.S. Tube	200	0	Working
7	20-13-2-X	165/60mA	1%	S.S. Tube	5	0	Working
7	20-14-3-F	180/100mA	1%	S.S. Tube	2	0	Working
8	20-9-1-L	180/100mA	1%	S.S. Tube	100	0	Working
8	20-9-1-T	245/50mA	1%	S.S. Tube	200	0	Shorted (Blunt)
8	20-6-2-H	265/50mA	1%	S.S. Tube	~100	0	Shorted
8	20-6-2-J	175/3mA	100%	S.S. Tube	15	0	Shorted
8	20-6-2-L	230/95mA	1%	S.S. Tube	2	0	Working
8	20-14-3-D	40/0mA	100%	S.S. Tube	0	Arc	Shorted

Table I (Continued)

Test Set	Cathode Number	Maximum V/I	Duty Cycle	Anode Type	Tips Blown	Arcs	Remarks
9	20-B-1-H	130/12mA	100%	S.S.	~ 500	0	Shorted
9	20-8-1-J	125/10mA	2%	S.S.	0	0	Working
9	20-8-1-M	190/100mA	1%	S.S.	~ 500	0	Working
9	20-8-1-N	120/10mA	2%	S.S.	3	0	Working
9	20-8-1-O	185/100mA	0.5%	S.S.	85	0	Shorted
9	20-8-1-P	125/10mA	2%	S.S.	0	0	Working
10	20-11-1-B	215/8mA	100	S.S.	500	0	Shorted
10	20-11-1-D	135/45mA	2	S.S.	~1000	1	Shorted
10	20-11-1-F	150/50mA	2	S.S.	0	0	Working
10	20-11-1-G	180/10mA	100	S.S.	~1000	0	Shorted
10	20-11-1-M	170/10mA	100	S.S.	110	0	Working
10	20-11-1-L	-	-	S.S.	-	-	Shorted
11	20-11-1-O	105/10mA	100	S.S.	-	0	Working
11	20-11-1-P	110/10mA	100	S.S.	-	0	Working
11	20-11-1-Q	130/2mA	100	S.S.	-	-	Shorted
11	20-11-1-T	-	-	S.S.	-	-	Shorted
11	20-11-1-V	-	-	S.S.	-	-	Shorted
12	20-42-2-P	215/80mA	2	S.S.	2	0	Working
12	20-42-2-O	240/8mA	100	S.S.	700	0	Shorted
12	20-42-3-J	-	-	S.S.	-	1	Shorted
12	20-42-3-G	-	-	S.S.	-	1	Shorted
12	20-42-3-F	-	-	S.S.	-	1	Shorted
12	20-42-2 T	-	-	S.S.	-	2	Shorted
13	20-42-3-I	-	-	S.S.	1	0	Shorted
13	20-42-3-N	185/40mA	2	S.S.	102	0	Working
13	20-42-3-O	220/25mA	2	S.S.	80	0	Working
13	20-42-3-S	140/35mA	2	S.S.	105	0	Working
13	20-42-2-M	220/50mA	10	S.S.	250	0	Working
13	20-42-2-S	200/40mA	10	S.S.	1500	0	Working
14	20-42-1-B	260/3mA	10	S.S.	~3000	1	Shorted
14	20-42-1-C	285/5mA	10	S.S.	~500	0	Shorted
14	20-42-1-D	320/30mA	10	S.S.	150	0	Working
14	20-42-1-F	280/10mA	100	S.S.	~200	0	Working
14	20-42-1-H	280/10mA	100	S.S.	85	0	Working
14	20-42-1-I	300/10mA	100	S.S.	250	0	Working
15	20-44-2-B	140/35mA	10	S.S.	40	0	Working
15	20-44-2-C	110/39mA	10	S.S.	50	0	Working
15	20-44-2-D	205/80mA	10	S.S.	16	0	Working
15	20-44-2-F	250/75mA	10	S.S.	14	0	Working
15	20-44-2-G	Short	100	S.S.	[illegible]	0	Shorted
15	20-44-2-F	250/90mA	2	S.S.	44	0	Working

Table I (Concluded)

Test Set	Cathode Number	Maximum V/I	Duty Cycle	Anode Type	Tips Blown	Arcs	Remarks
16	20-44-2-I	215/35mA	10	S.S.	~300	2	Shorted
16	20-44-2-K	Short	100	S.S.	0	0	Shorted
16	20-44-2-L	260/50mA	2	S.S.	21	0	Working
16	20-44-2-M	265/5mA	100	S.S.	~700	1	Shorted
16	20-44-2-N	245/10mA	100	S.S.	75	0	Shorted
16	20-44-2-O	255/30mA	10	S.S.	100	0	Working
17	20-45-2-F	105/35mA	10	S.S.	1	0	Working
17	20-45-2-G	130/40mA	10	S.S.	2	0	Working
17	20-45-2-L	110/20mA	100	S.S.	0	0	Working
17	20-45-2-O	105/30mA	10	S.S.	0	0	Working
17	20-45-2-P	130/50mA	10	S.S.	0	0	Working
17	20-45-2-Q	130/15mA	100	S.S.	0	0	Working

Test set 2, in Table I, represents the first trial in which the stainless steel tube collectors were used. All of the cathodes of this test set were damaged by an arc except 20-9-2-m, which was tested to 50 mA and found to have only one tip damaged. Some time after this test we discovered damage to the cathodes caused by the discharging of a capacitor in the driving circuit through a temporary base-to-gate short. This arcing clouded the results and the performance of the stainless steel tube collector at that time did not seem to be significantly different from that of the molybdenum collector (set 1), and thus tests continued using copper collectors for sets 3, 4, and 5. After test set 5 it was clear that the copper collectors were not going to be satisfactory for this work. It was also clear that the capacitor in the circuit caused the arcs which damaged the cathode structure in sets 1 and 2.

Thus the decision was made to reexamine the stainless steel tube collectors with the offending capacitor removed from the driving circuit. The results (set 6 of Table I and Figure 13(c)) were dramatic: there were no arcs and two cathodes achieved the goal of 95 mA or more. Of the next 12 cathodes tested (sets 7 and 8), nine achieved 50 mA or higher and six achieved the goal of 95 mA or more.

The remaining difficulties seem to be associated with space charge effects in the beam that lead to bombardment of the gate film at high emission levels. For the purposes of this phase of the program these results are satisfactory and the question of collector design and processing was not pursued further. It is clear, however, that more work must be done with the collector arrangement if the cathode's full potential with respect to reliability and maximum output current is to be realized.

D. Cathode Geometry

1. Tip Geometry

As noted in the introduction, Fowler-Nordheim theory shows that emission current increases exponentially as the field increases. The field at the tip depends on factors which include the tip radius (r) and the distance (R) between the tip and the counterelectrode, or gate film in the case of the TFFEC.

A pattern emerged as observations were made of cathode performance as a function of hole radius (R), tip radius (r), and cone height: hole radius and cone height seemed to have a strong effect on current obtained for a given voltage but tip radius seemed to have little effect. For example, Figure 16 shows two emitters with tip radii differing by approximately a factor of 4, but with tip height and hole size very nearly the same. According to theory, the field at the tip is roughly inversely proportional to the tip radius so we should expect the voltage requirement to increase by a factor of 4 to compensate for the reduced field enhancement of the blunter tip. The voltage required to produce 10 mA from the

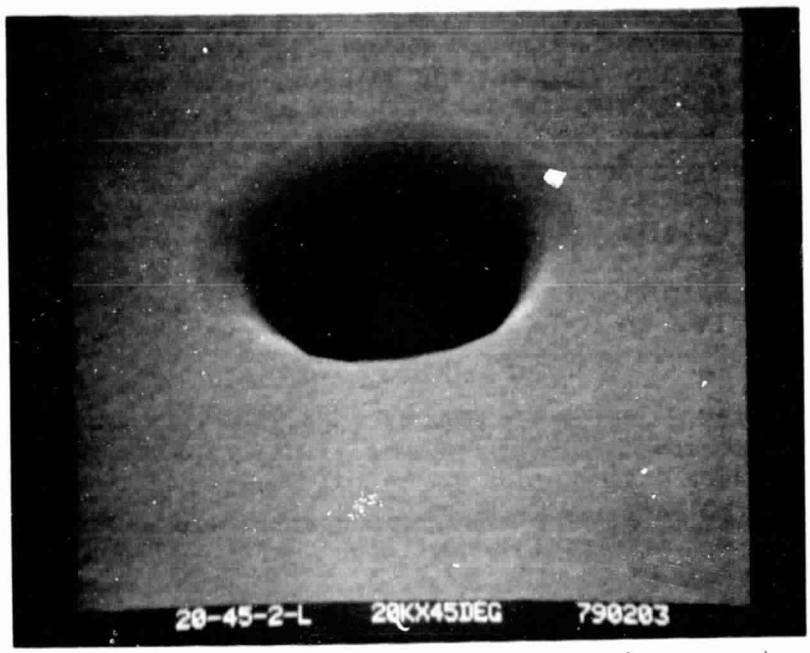

(a) 10-mA EMISSION AT 100 VOLTS ⊢— 1 μm —⊣

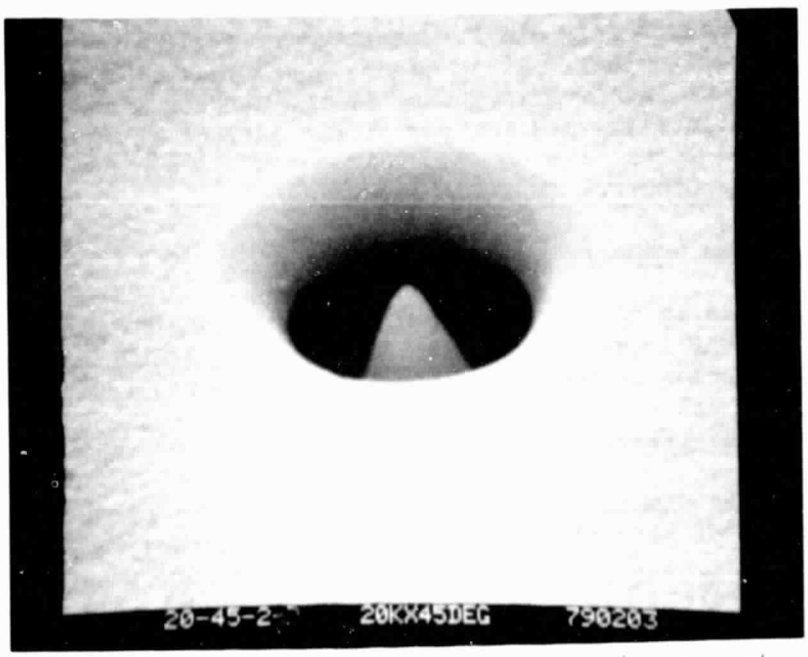

(b) 10-mA EMISSION AT 90 VOLTS ⊢— 1 μm —⊣

FIGURE 16 EMISSION FROM TIPS OF DIFFERENT RADII

sharper tip cathode was 100 volts, and the blunt tip cathode produced 10 mA with an applied voltage of 90 volts. This is surprising, and not consistent with theory at first thought.

A possible explanation is that the emission actually is dependent on work function modification by adsorbates and field enhancement caused by tip surface microstructure which has dimensions of a few angstroms. Gomer[5] describes just such a mechanism: "Surface irregularities of very small size will show up as bright magnified regions (in a field emission microscope) if the local work function and field compare favorably with the surroundings, that is, if

$$(\phi^{3/2}/F)\ \text{bump} \cong (\phi^{3/2}/F)\ \text{tip}.$$

This condition is often met by individual molecules, or small clusters, and by oriented overgrowths a few atom layers in thickness or width."

Data gathered in a study in this laboratory of noise in field emission[6] support the liklihood of the emission emanating from small areas on the tip. The results of this study can be briefly summarized as follows:

(1) The emitting areas computed by the Fowler-Nordheim method are on the order of a few square angstroms.

(2) If a "smooth" spherical cap tip is assumed, the calculated electric fields at the tip are too small by a factor of 4 to account for the emission observed without assuming an unreasonably low work function for the surface.

(3) On the basis of a linear variation of work function with the field[5], the apparent area reduction is too large to be obtained without a substantial deviation from the Fowler-Nordheim relationship. No such deviation was observed.

(4) Images observed in a field emission microscope usually consist of "lobes" without the regular pattern seen with clean single crystal emitter tips.

(5) Burst noise occurs in pulses of equal height with rapid rise times and is indicative of atomic effects such as the rearrangement of atoms at the tip.

Microstructure and surface conditions that modify the effective work function of the tip dominate. Therefore, these experiments have not shown differences in performance that can be attributed to tip radius alone. Section E discusses in more detail the results of some experiments dealing with surface effects.

2. Hole Geometry

The hole diameter is the main dimension controlling tip-to-counter-electrode spacing. The best results with respect to voltage required for a given level of emission have been obtained with small hole diameters and with cone heights that place the tip in or slightly above the plane of the counterelectrode. However, for the reasons discussed above, and in the next section, it has not been possible to obtain definite and consistent data on preferred geometries.

E. The Effects of Environment on Cathode Emission

1. Pressure Environment

A study of pressure effects on cathode performance was beyond the scope of this program; however, one of the experimental setups provided an opportunity to make some observations with essentially no extra effort. The vacuum system used to set up an electron optics bench included a gate valve between the chamber and the ion pump. Thus it was possible to measure the pressure in the chamber with an ion gage while changing the pressure in a controlled fashion by throttling the pump with the gate valve.

A cathode was set up in a gun configuration with a phosphor for viewing the beam shape as shown in Figure 17. The chamber was pumped to 1×10^{-9} torr without bakeout and a series of tests performed with the lens system (discussed in a later section).

The cathode was then set at an emission level of 20 μA, as measured at the phosphor, and observed to be stable at that level for 150 hours at room temperature. During this time the applied potentials were 115 V on the cathode and 6 kV on the phosphor and accelerating lens. The pump was then throttled by partially closing the gate valve. The pressure in the chamber was monitored with an ion gage and set to 1×10^{-5} torr by adjusting the gate valve. The emission was observed over the next 360 hours with a constant voltage of 115 V on the cathode. As shown in Figure 17, the emission fell to a level of 1.5 μA over a period of about 230 hours and remained essentially at that level for the next 130 hours. At the end of that time the gate valve was again opened and the pressure dropped very rapidly to 1×10^{-9} torr. The emission from the cathode increased to the original value of 20 μA over a period of 50 hours and remained at that level for another 100 hours before it was turned off and the system opened for a change in the gun structure. An examination of the cathode revealed no detectable damage as a result of this experiment

Qualitatively, these results are as expected[7], but as far as we know this type of measurement has never before been performed at these pressures. Measurement of gas adsorption effects is usually done on "clean"

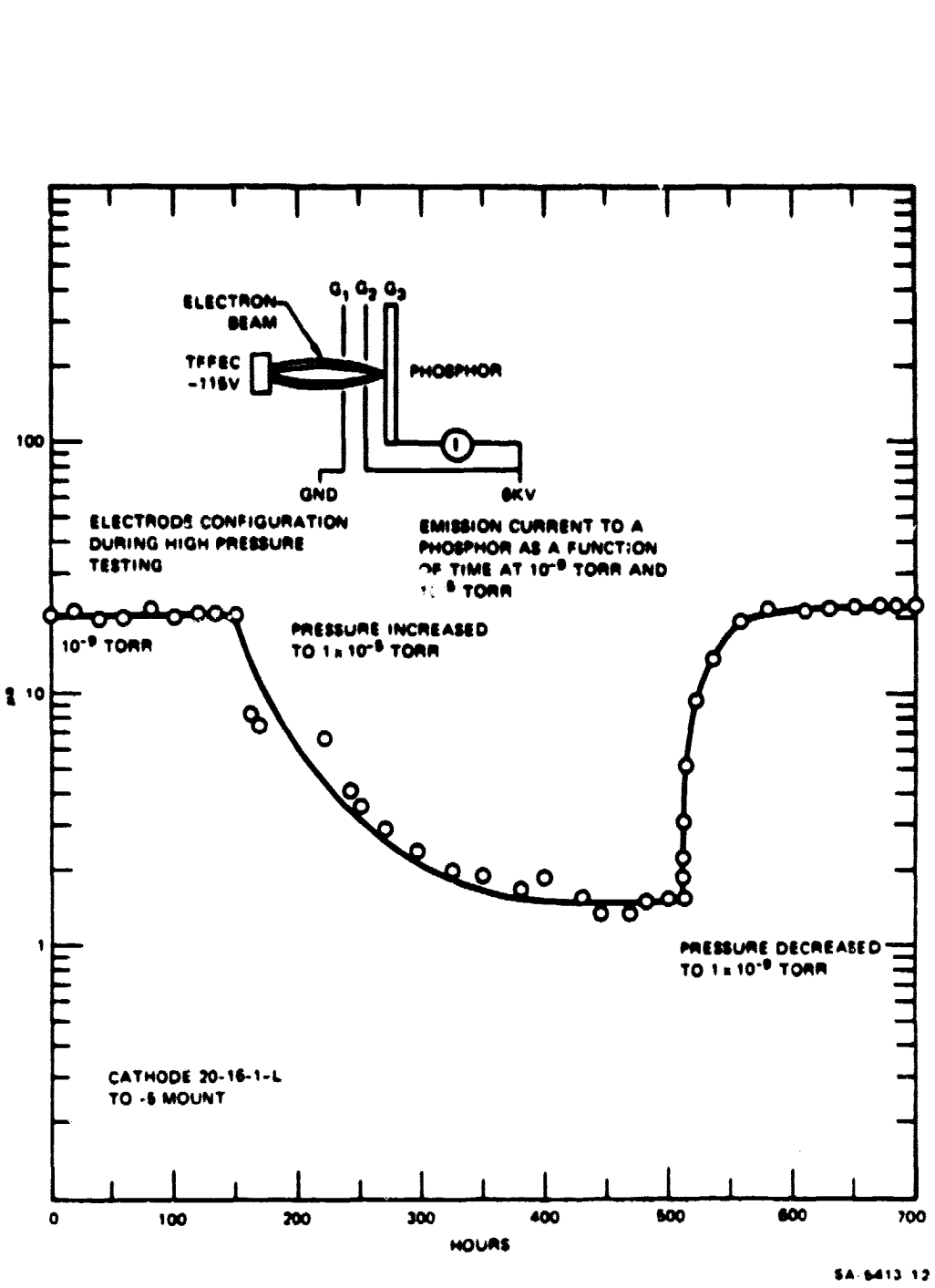

FIGURE 17 EMISSION DEPENDENCE ON BACKGROUND PRESSURE AND TIME

tips in the 10^{-9} torr region, i.e., four orders of magnitude lower than our operating pressure. A later program supported by NASA through the Jet Propulsion Laboratories (SRI Project PYD 6932, JPL Contract No. 954840, subcontract under NASA Contract NAS7-100) added more interesting results to the high pressure investigation. Under this program the effects of several gases on cathode performance at room temperature were observed. These gases were Ar, Ne, He, H_2, NH_3, CH_4, H_2S, and H_2O.

Briefly, the results show that with the voltage held constant, the emission was essentially unchanged by Ar, Ne, and He, but was increased by H_2, NH_3, CH_4, H_2S, and H_2O. Figure 18 shows 10^{-6} torr of H_2 and H_2O to illustrate the nature of the effect. The initial drop in emission when the water leak was introduced is believed to be caused by air trapped in the water sample. In all cases the effect was completely reversible, and therefore is thought to be due to adsorption and desorption of gases on the tips with a corresponding change in the effective work function of the tips. It would then be reasonable to assume that O_2 in air is responsible for the emission decrease when air is introduced to the system, since O_2 is electronegative. Figure 19 shows that this is indeed the case.

Another interesting effect of O_2 is the extremely quiet emission obtained when the cathode came to equilibrium with the O_2-rich environment. This result could be important in applications where very stable emission is required.

These experiments were preliminary in nature and intended only to show trends. Therefore, it was not possible to study more gases or the effects of temperature, various emission levels and any changes in the emission patterns when operating under these conditions.

2. Temperature Environment

As discussed earlier, operation of the cathode at current levels in the 15-mA range at a 100% emission duty cycle was seen to cause the stainless-steel tube collector to heat to incandescence (~ 800 to 900°C). When this was first observed, the emission was immediately reduced to prevent damaging the cathode or collector.

More recently an experiment was performed during which the collector heated to these temperatures during bombardment from an emitter array while no operator was present. The cathode had been left at 190 volts with 10-mA emission at 100% duty cycle. Forty minutes later the operator returned and noticed that the emission current was off scale (over 16 mA), and the voltage had dropped to about 75 volts due to protective series resistors in the circuit. The voltage was reduced and the cathode was seen to require only 65 volts to produce 10 mA emission. This level of emission was maintained for at least three hours, and the cathode was left operating at this voltage over night.

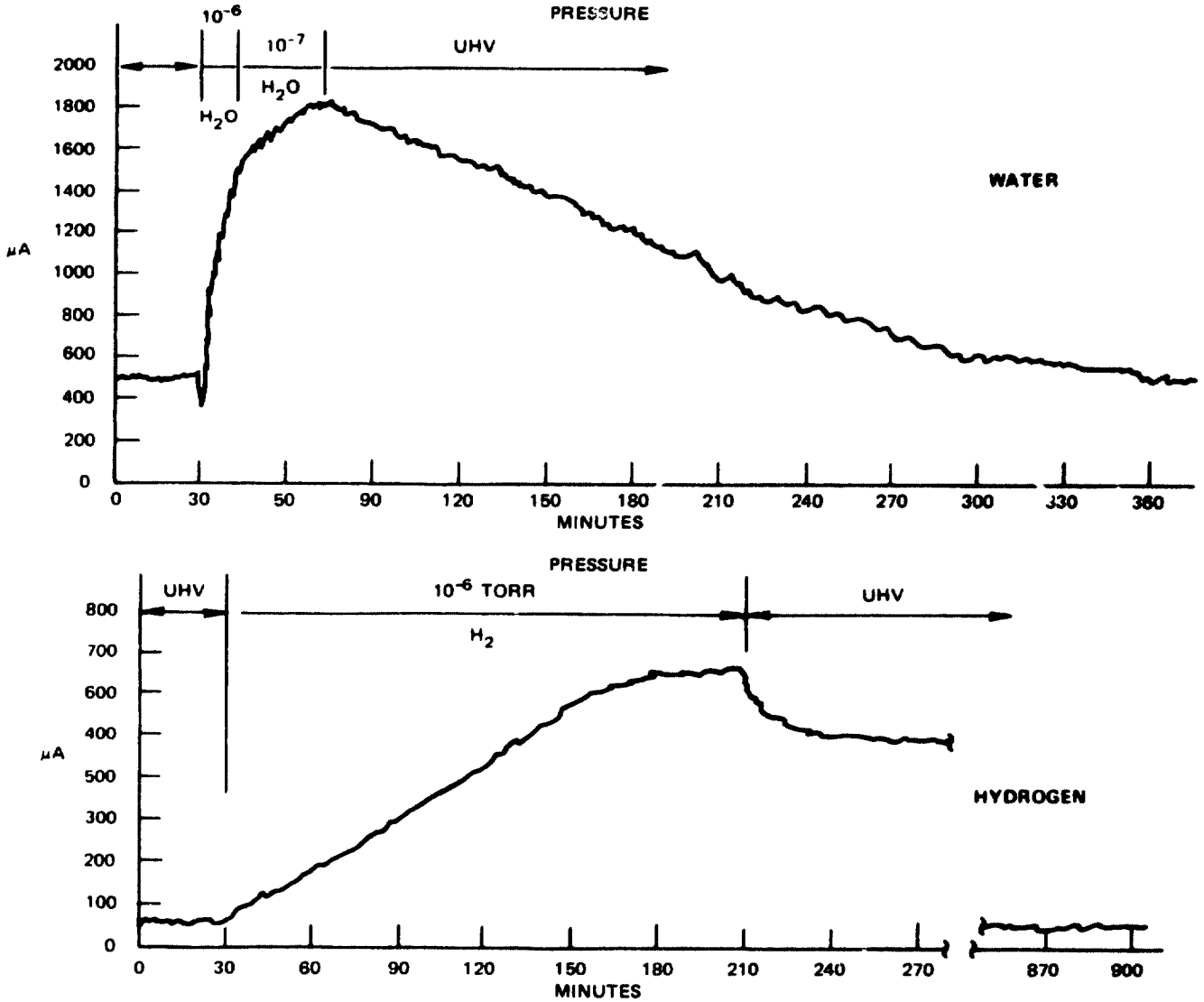

FIGURE 18 EMISSION BEHAVIOR AS A FUNCTION OF TIME IN WATER VAPOR AND HYDROGEN

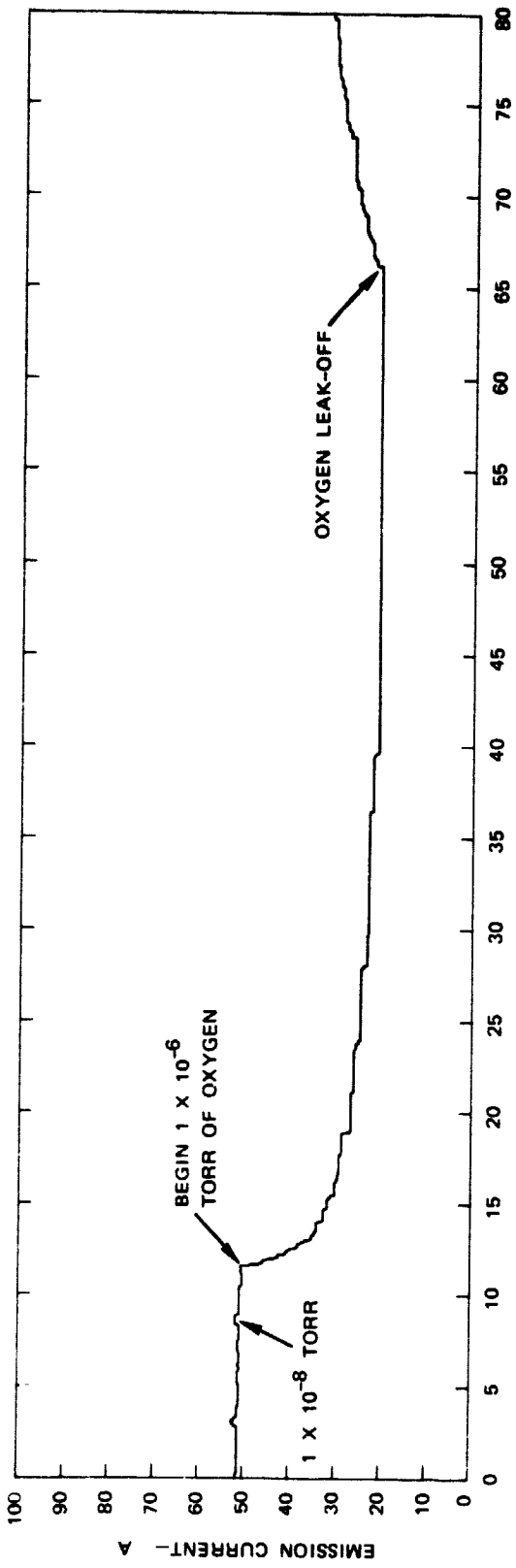

FIGURE 19 THE BEHAVIOR OF EMISSION CURRENT IN 1 X 10^{-6} TORR OF OXYGEN; VOLTAGE HELD CONSTANT

The following morning the cathode required 105 volts for 10 mA; after two days it required about 115 volts. Figure 20 shows the results on a Fowler-Nordheim plot. That the effect is reversible and the slopes of the curves are different suggests the shift in characteristics is caused by an effective change in work function by desorption from the tips, or perhaps by adsorption of material from the collector: It does not seem to be due to a geometrical change such as roughening or sharpening of the tip by sputtering. This result is recent and incomplete, but 10 mA of field emission at 65 volts is very attractive and certainly worth pursuing.

From these results it is clear that the previous attempts to make sense of the effects of geometry on the emission characteristics of a cathode were futile without careful control of the cathode's environment. The surface condition of the tips is the likely cause of an apparent contradiction (sharper tips require more voltage to produce a given current) as shown in Figure 16. The sharper cathode might produce higher emission levels than the larger-radius cathode if the two were operated under identical conditions; or it may be that microstructure dominates the situation under those conditions, and the blunt tip produces more emission because of a larger effective emission area.

We stress, however, that with the exception of the consistently poor results with cathodes whose cone height places the emitter tip below the plane of the counterelectrode, results obtained to date have not yielded a preferred geometry.

F. Lifetime Tests

Life studies were initiated on the previous cathode program (NASA Contract NAS3-18903). Three 100-tip-array cathodes were sealed in separate stainless-steel tubes with 2 liter/sec appendage pumps. The cathodes were originally set at peak 60-Hz emission levels of 2 mA (3 A/cm^2) in the middle of March 1975. Since that time, many events have influenced the performance of the three cathodes. One of them was severely damaged by a collector power supply failure on March 2, 1978, and subsequently failed to a short circuit between the gate and base on March 27, 1978. This cathode operated at levels of 1 mA to 2.25 mA for a total of more than 3 years (26,000 hours).

The other two cathodes are still operating and in December 1978 had more than 33,000 hours of total time at emission levels between 2.5 and 1.5 mA. Figure 21 shows one of the cathodes at the start of the test on March 7, 1975 and (after approximately 33,000 hours) on December 11, 1978. The emission has not been steady at 2 mA as shown throughout that time; but from the lack of more than very small changes in the voltage-current characteristic, it is not likely that any of the power failures that the experiment suffered caused any permanent damage. All of the large emission changes have been associated with power supply failures that caused voltage transients or bombardment of the gate film induced by a collector bias failure.

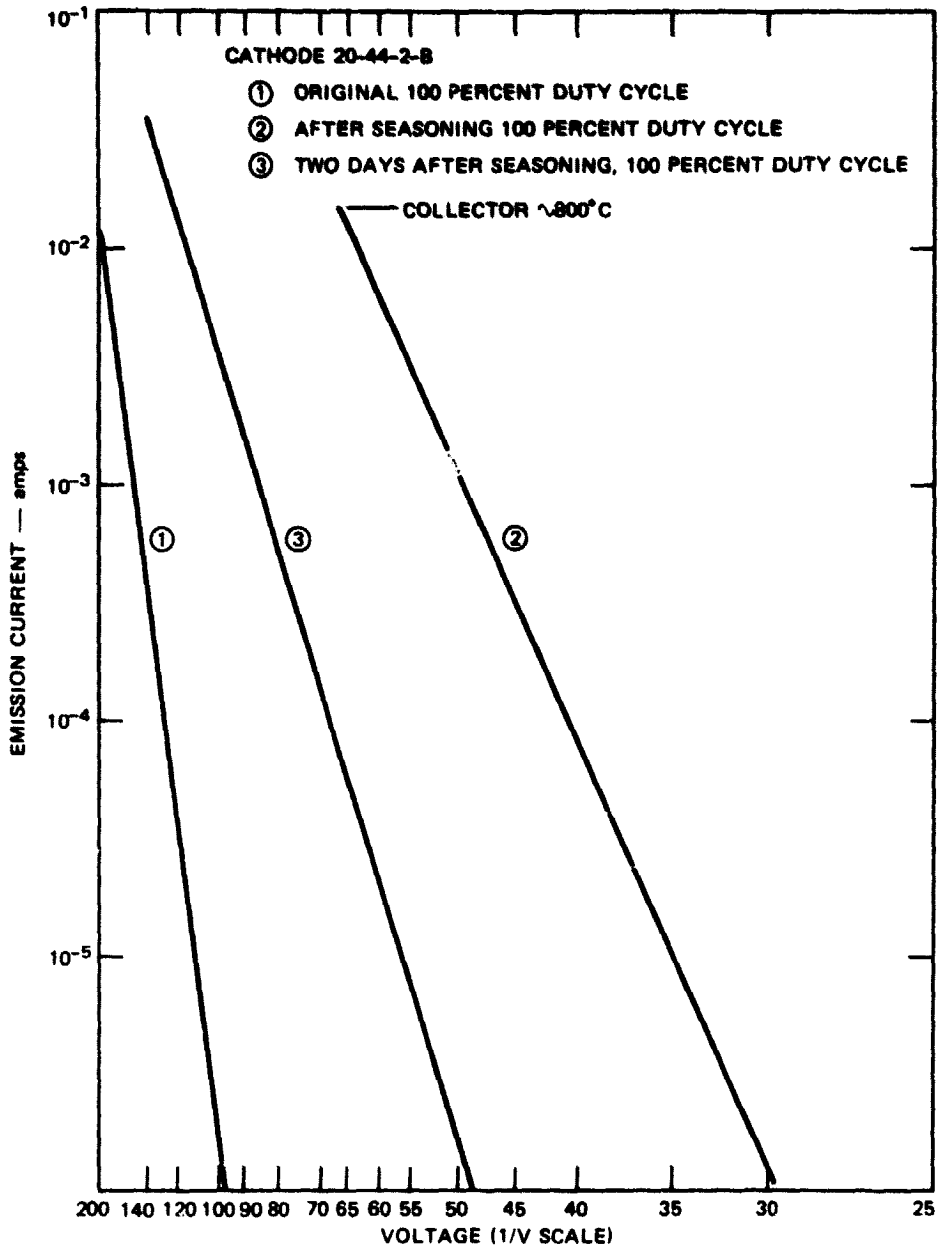

FIGURE 20 FOWLER-NORDHEIM PLOT OF EMISSION CHANGES AT HIGH POWER LEVELS

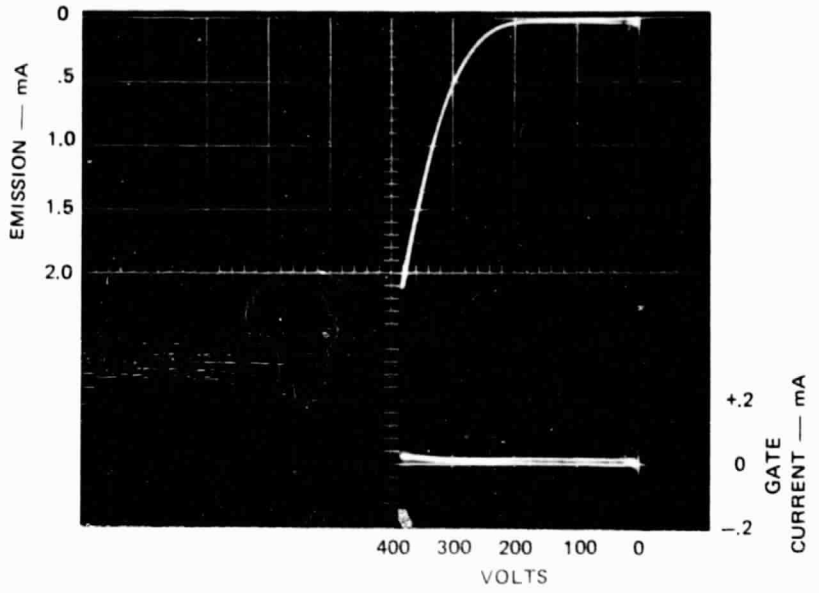

(a) START OF LIFE TEST (MARCH 7, 1975)

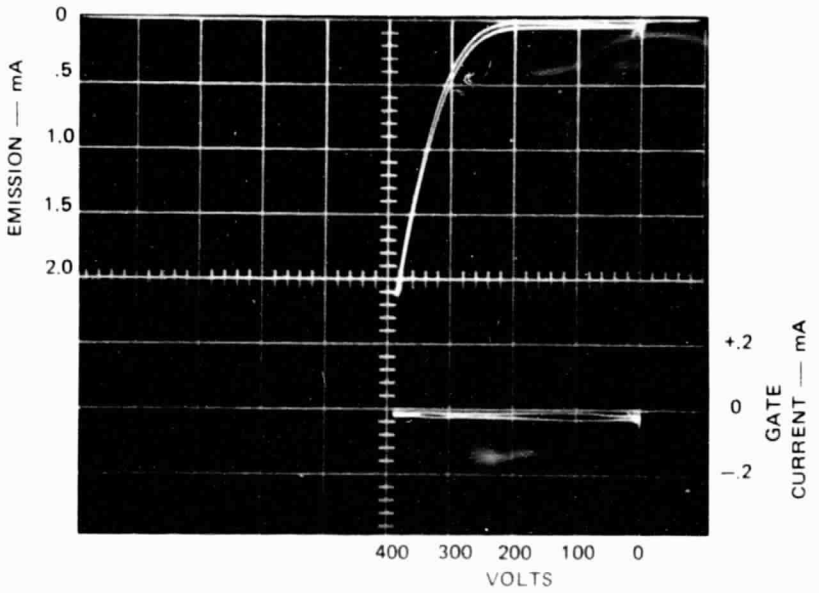

(b) EMISSION AFTER 33,000 HOURS (DECEMBER 11, 1978)

FIGURE 21 CURRENT-VOLTAGE OSCILLOGRAPHS FOR 100-CONE ARRAY DRIVEN BY A 60-Hz HALF-WAVE VOLTAGE TO A PEAK CURRENT OF 2-mA FOR 33,000 HOURS

The cathodes seem to recover slowly after a disturbing event such as a bias failure, and the effect seems to be much like that observed with the high pressure tests. It may be that a bias failure leads to bombardment of the tube walls and outgassing that results in an increase in work function of the tips; after the bias is restored, the tips slowly clean up again.

G. Energy Spread

The energy distribution of field emitted electrons has been investigated[8,9,10] and is generally accepted to be similar to that of a thermionic cathode when the field emitter is operated at room temperature. That is, the usual data show a half height width of about 0.2 eV. These measurements are difficult to perform and they require carefully constructed apparatus of the sort used by van Oostrom[9] shown in Figure 22. An Einsel lens is used to focus the beam on a point which is at the center of curvature of a hemispherically-shaped collector. Then, since the beam will travel radially from the focal point, it will in theory approach the collector without having any energy component parallel to the surface of the collector. [11]

Figure 22 shows how measurements were made with the apparatus. Voltages are applied to the lens as shown and the tip bias is set to about -30V. The cathode driving voltage is then adjusted to produce the desired level of emission to the collector. A ΔV is then applied to the tip bias in the form of a 0.6 volt peak-to-peak square wave. The total energy distribution can then be measured by varying the cathode voltage from zero to -30 V and by measuring the total current to the collector and the relative slope of voltage current curve from the amplitude of the ac component of the collector current. The normalized differential curve shown in Figures 23 and 24 is the usual display form of energy distribution data.

Figure 23 shows the results obtained by setting V_1 at 5 kV, the maximum emission at 1.6 μA, ΔV at 0.6 V peak-to-peak, and tuning V_2 to give the best peak definition while sweeping the tip voltage (V_k) through a range of several volts. Curve 1 is the dc component of the emission current. The threshold for the onset of collector current is 4.5 volts, consistent with published values for the work function for the molybdenum collector. The emission appears to fall off at values of tip voltage above about -19 volts, as reflected electrons are lost from the collector. The differentiated curve (2) is rather unusual: it shows many peaks rather than one as is seen with single tip emitters. At first thought this would be interpreted to mean that there are voltage differences between the emitting tips.

The mechanism for such voltage difference is not apparent. For example, Figure 24 shows the results obtained by setting the emission level

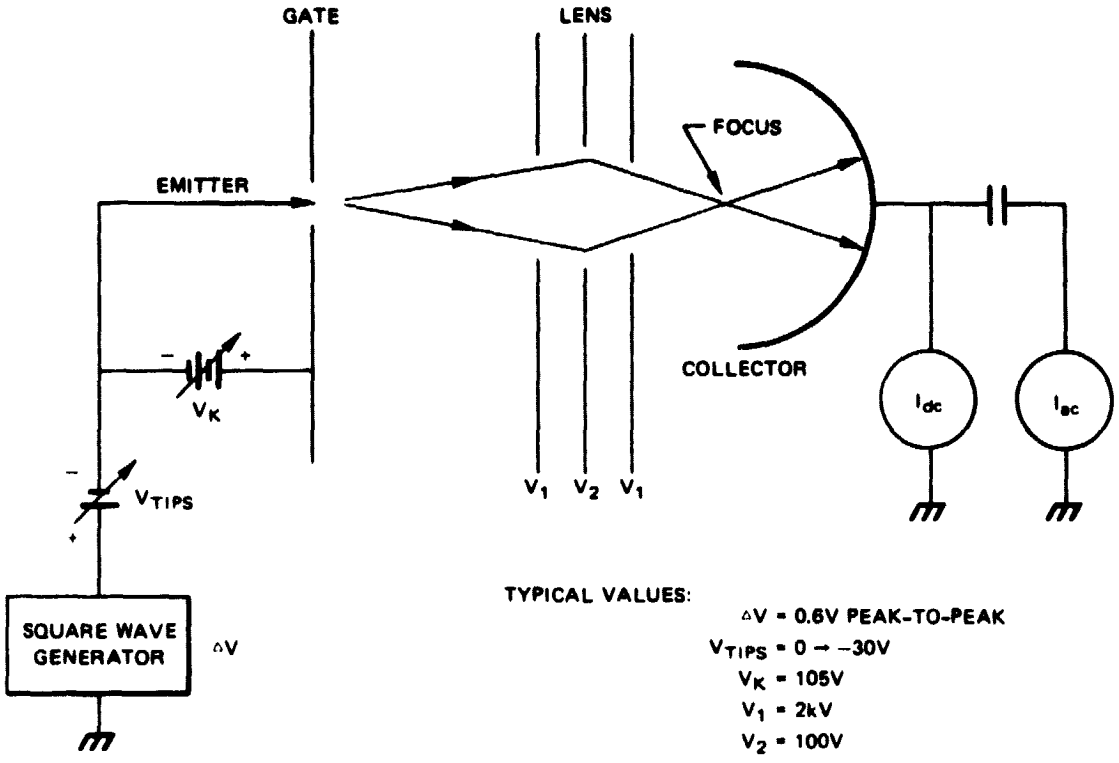

TYPICAL VALUES:

ΔV = 0.6V PEAK-TO-PEAK
V_{TIPS} = 0 → −30V
V_K = 105V
V_1 = 2kV
V_2 = 100V

FIGURE 22 TOTAL ENERGY DISTRIBUTION SETUP

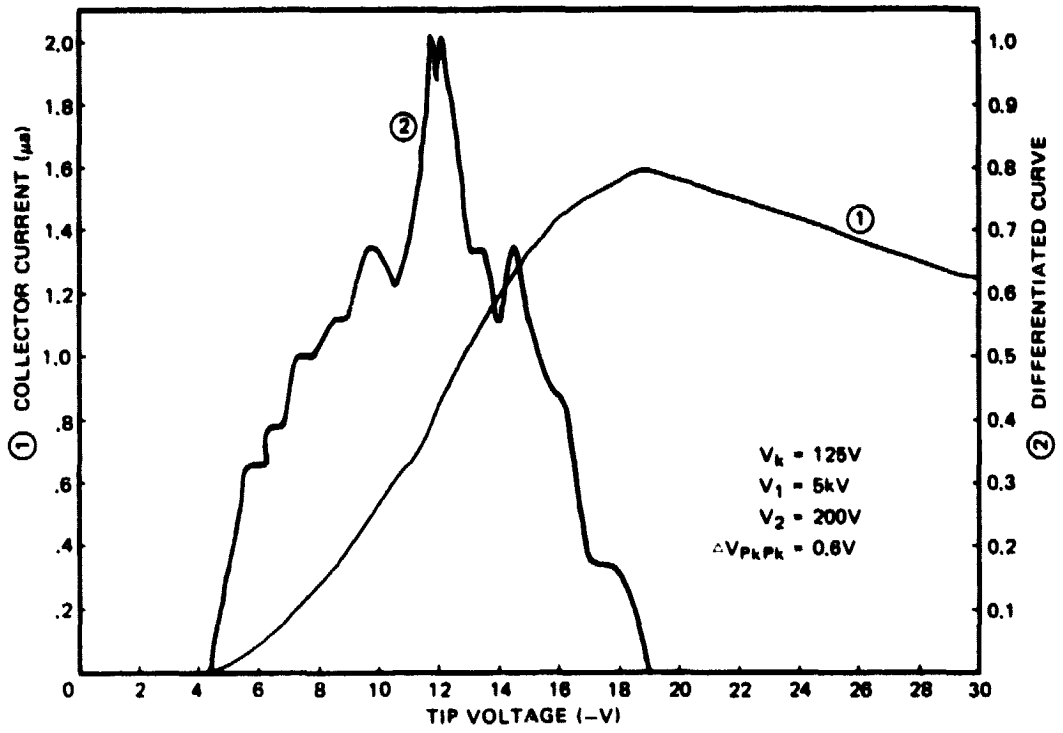

FIGURE 23 COLLECTOR CURRENT AND DIFFERENTIATED COLLECTOR CURRENT AS A FUNCTION OF TIP VOLTAGE (V_k = 125, V_1 = 5k, V_2 = 200)

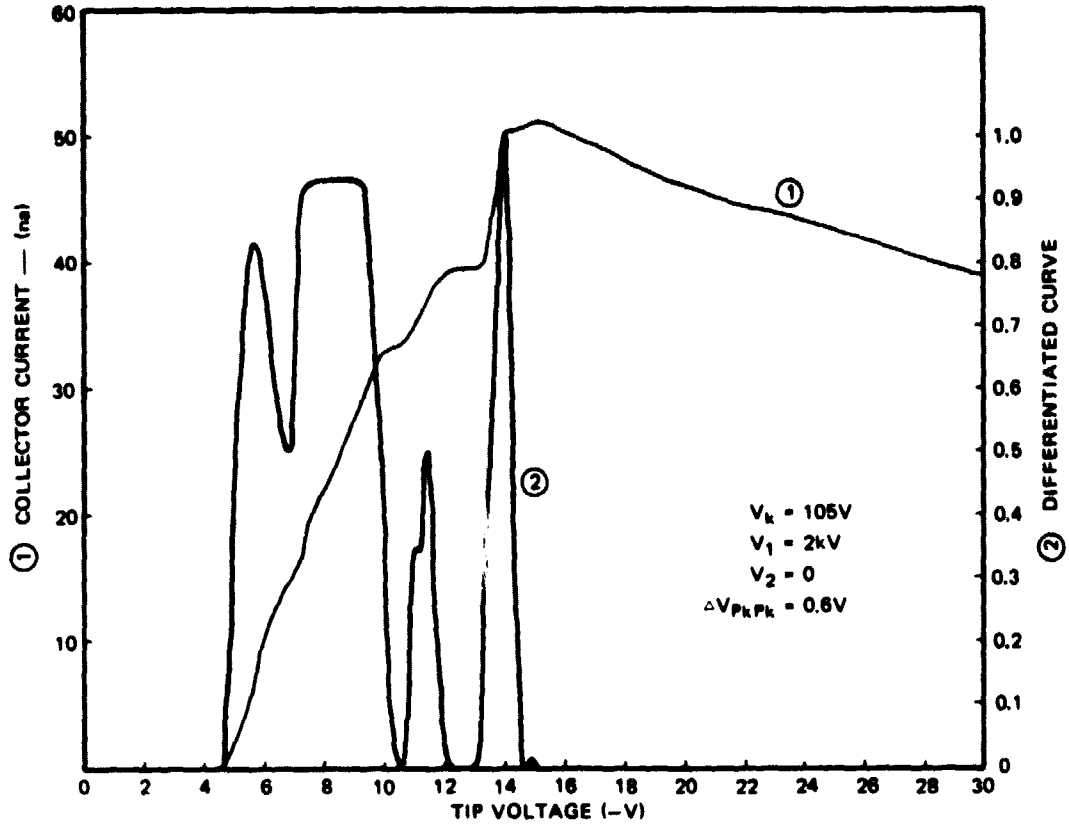

FIGURE 24 COLLECTOR CURRENT AND DIFFERENTIATED COLLECTOR CURRENT AS A FUNCTION OF TIP VOLTAGE (V_k = 105, V_1 = 2k, V_2 = 0)

at ~ 50 nA and tuning the voltages for the best peak resolution on the dI/dV curve. There is a 10-nA current rise in the current curve with a correspondingly large peak in the dI/dV curve at about 14 volts, or about 9 volts higher than the onset of current flow to the collector. This would imply a 9-volt drop in series with the tip that was responsible for that 10 nA of emission, and the effective resistance in series with that tip would then have to be 900 megohms or about 10^9 ohms. If one were to assume that a 1-μm cylinder 1-μm long under the cone was responsible for this resistance (a conservative estimate), its resistivity would have to be ~ 10^5 Ω-cm to account for such a high impedance. This would be difficult to attain in the 0.01 Ω-cm silicon used as the base material.

A more likely explanation is the electron optics of the situation; emitter tips off the optical axis or perhaps emitting at a difficult angle may be responsible for the spread, since the system is designed for a single, on-axis emitter source. It is possible that the optics of our apparatus were not good, but we note with interest that similar experiments (unpublished) by van Oostrum using the apparatus described in Ref. 9 produced equivalent results.

H. Electron Optics Tests

1. Approach

The ultimate goal of the program is to produce a 95 mA, 0.26-mm diameter beam at a position 2.51 cm from the cathode surface. The usual approach to a gun system design problem would be to set up a computer model and plot electron trajectories for various electrode configurations. Many electronoptics design problems are amenable to such analysis by direct computer methods; the voltage equipotentials are derived from a given electrode configuration and then used to compute the electron trajectories. Generally, such computations are handled in two parts: the first-order properties of the system (focal points, principal planes, and image points) are derived as an initial step; using this information, the trajectories can be computed to higher accuracies by introducing aberration terms. Most electron-optics systems have electron beams that deviate only slightly from the system's axis, and the trajectory angles (measured from the axis) remain quite small, usually smaller than 0.01 radian or about 0.5%. These small angles make it possible to obtain good trajectory approximations by using third-order aberration theory and neglecting all higher orders.

An electron gun using the TFFEC however, utilizes beams which may have positions far from the system axis and angles of at least 10° and perhaps as high as 30°. In these circumstances accurate computer calculation techniques are difficult to use. Thus the initial work was planned with a more heuristic approach, employing minimum digital computation. This approach was divided into three separate parts:

- An analogy modeling system based on a two-dimensional rubber membrane table.
- Simple electron-optics computer calculations for the cathode region of the gun.
- A flexible, high-vacuum electron-optics test bench to define the final gun design.

A NASA trajectory program was used later to trace rays in gun configurations that emerged from these investigations; first tests used Kleynen's[12] rubber membrane model.

2. The Rubber Membrane Model

Kleynen's rubber membrane model represents electrodes with various voltages as elevational changes in a stretched rubber-membrane sheet. The combination of gravity and the impressed electrode shapes causes small balls on the sheet surface to roll in trajectories in direct analogy to electrons moving in the electric field produced by similarly-shaped electrodes. Unfortunately the analogy is precise only for two-dimensional (planar) systems, and we are considering a rotationally-symmetrical three-dimensional system. Even with this restriction, however, there is a good qualitative analogy between the two-dimensional and the three-dimensional results. This was sufficient similarity: in the initial stage of the work we were looking only for trends, generalizations, and approximations. For example, we wanted to understand the general influence of different electrode shapes, hole diameters, and electrode positions on final beam spot size.

The rubber membrane table was initially set up as shown in Figure 25. The electrodes were shaped from wood and positioned with appropriate clamps on the table frame. The rubber membrane was painted black for visual contrast with the 3/8-inch steel ball bearings which were rolled on the surface to trace out trajectories.

The first tests established the experimental procedure and obtain repeatable results. This presented no difficulties, but we did find it necessary to observe a few precautions. For example the launching of the balls onto the table had to be done carefully and repeatably with no bounce or skidding as the ball travelled from the launch ramp to the rubber surface. Fabrication of a simple launching device was required as hand-held mechanisms were not accurate enough. The launcher consisted of an aluminum ramp with a 7° slope and a groove to guide the ball leading down the slope. The launch velocity (cathode tip voltage) was varied by changing the distance up the ramp from which the ball was launched. The ball was held in place on the ramp before launch by a small suction tube mounted on the ramp and on axis with a line parallel to the ramp and through the center of the ball. The ball was launched by placement on the ramp against the

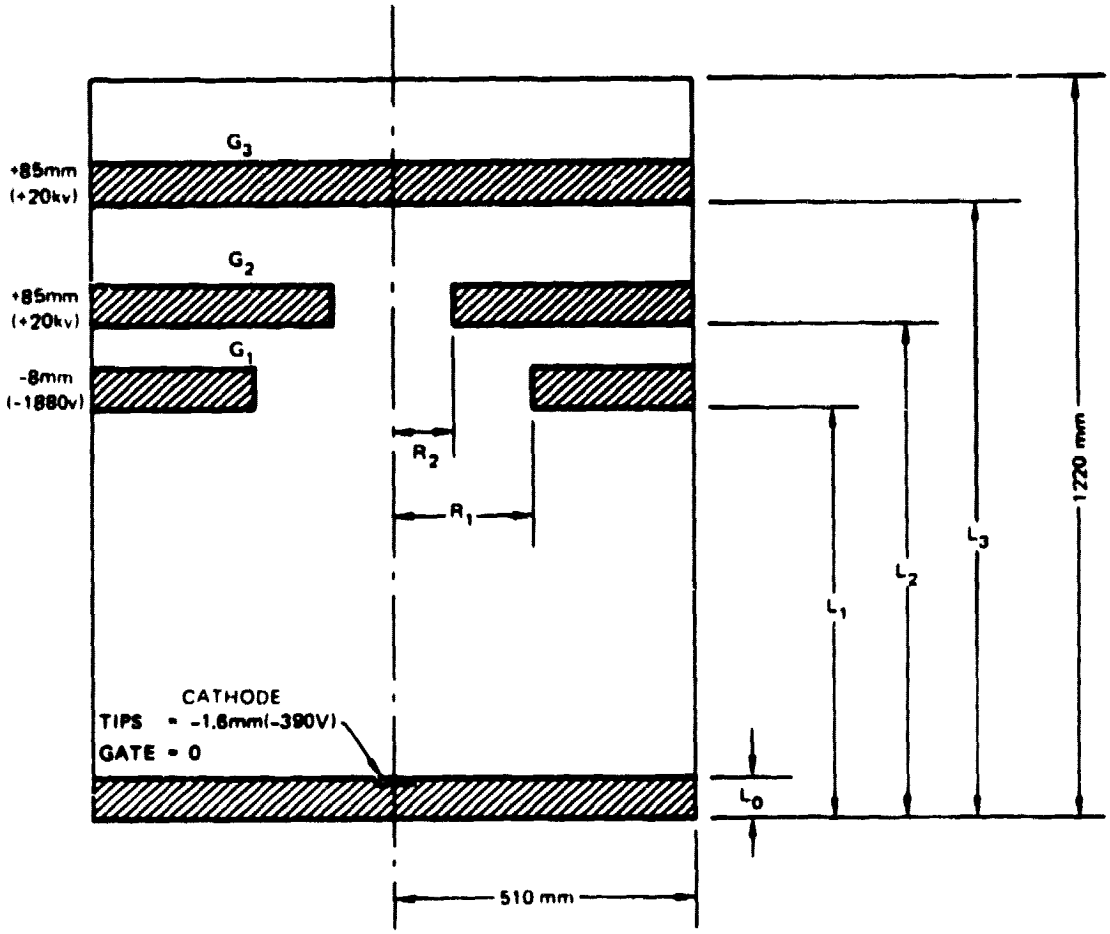

FIGURE 25 PLAN VIEW OF THE RUBBER-MEMBRANE TABLE SHOWING ONE OF THE ELECTRODE CONFIGURATIONS USED

Table frame (border) was taken as 0 elevation and distance up as (−) and distance down as (+).

suction tube with suction applied. The suction was then interrupted, releasing the ball to roll down the predetermined length of ramp and onto the rubber surface. The trajectory of the ball on the surface was traced by darkening the room and while illuminating the ball with a flashlight, photographing the table with a time exposure camera mounted directly over the table. The angle of launch was varied over $\pm$ 30° from the axis of the electrode system; the position was varied over a distance to the left and right of the axis that was proportional to the 0.5 mm radius of the TFFEC's active area. Several experiments showed remarkable repeatability with this setup if one was careful to keep the balls and table clean--even using gloves or a clean tool for handling the ball bearings. Figure 25 shows typical electrode elevations (voltages) with respect to the table frame which was taken as zero or ground. Table II shows other configurations tested.

Ball (electron) velocity was measured using a strobe light during the time exposure and measuring the distance between successive ball images. The distance (D) between ball images is proportional to the ball velocity (D/t), and the surface elevation or potential (V) is proportional to the square of the ball (electron) velocity, i.e.,

$$qV = 1/2\ m(D/t)^2 \tag{5}$$

where q = the electronic charge, V = potential, m = electron mass, and D = distance traveled in time(t).

Thus, by measuring the distance (D_3) between ball images at the target electrode (G_3), and assigning a voltage (V_3) to the elevation of G_3 relative to the cathode gate, the voltage at any other point in the trajectory (V_x) can be found by measuring the distance between ball images (D_x) and using the equation

$$V_x = V_3\left(\frac{D_x}{D_3}\right)^2 \tag{6}$$

Using this technique, the cathode (tip) potential, or launch velocity, was determined to be 650 V when the target voltage was 20 kV. This was then assumed to be a reasonable (i.e., an upper limit that would never be exceeded) value for a cathode operated at 100 mA. Later the launch was lowered to 390 V and the most recent cathode data shows that $\sim$ 200 V is sufficient for 100 mA in most cases.

Table II is a tabulation of the configurations used for time photographs of ball trajectories. Balls were usually launched from three positions on the scaled cathode surface: the center, the left edge, and the right edge. They were also launched at three angles from each position, 0°, +30°, and -30° from the normal to the surface. Figure 26 demonstrates photographically the techniques and the results. The first several trials were to establish the techniques of lighting, photography, launching, and to determine the sensitivity of the experiments. As illustrated in Figures 26(a) and 26(b) (No. 15 and 16 in Table II), sensitivity to electrode

Table II

RUBBER MEMBRANE TEST DATA

No.	L_0	L_1	L_2	L_3	G_0	G_1	G_2	G_3	R_1	R_2	Launch Angle	Launch Point
1	60	575	750	965	-2	-25	+85	+85	250	120	0 ± 10 ± 20 ± 30	0
2	60	575	750	965	-2	-25	+85	+85	250	120	0 ± 30	0 ± ½
3	60	575	750	965	-2	-25	+85	+85	250	120	0 ± 10 ± 20 ± 30	0
4	60	575	750	965	-2	-38	+85	+85	250	120	0 ± 30	0 ± ½
5	60	575	750	965	-2	-38	+85	+85	250	120	0 ± 30	0 ± ½
6	60	575	750	965	-2	-38	+85	+85	250	120	0 ± 30	0 ± ½
7	60	575	750	965	-2	-38	+85	+85	250	120	0 ± 30	0 ± ½
8	60	575	750	965	-2	-13	+85	+85	250	120	0 ± 30	0 ± ½
9	60	290	750	965	-2	-25	+85	+85	250	120	0 ± 30	0 ± ½
10	60	290	750	965	-2	-25	+85	+85	220	120	0 ± 30	0 ± ½
11	60	575	750	965	-2	-19	+85	+85	260	120	0 ± 30	0 ± ½
12	60	575	750	965	-2	-19	+85	+85	260	120	0 ± 30	0 ± ½
13	60	575	750	965	-2	-25	+85	+85	260	120	0 ± 30	0 ± ½
Launcher modified to eliminate slight bounce.												
14	60	575	750	965	-2	-25	+85	+85	260	120	0 ± 30	0 ± ½
15	60	575	750	965	-2	-38 Rt -40 Lt	+85	+85	260	120	0 ± 30	0 ± ½
16	60	575	750	965	-2	-40	+85	+85	260	120	0 ± 30	0 ± ½
17	60	575	750	965	-2	-40	+85	+85	260	120	0 ± 30	0 ± ½
18	60	575	750	965	-2	-40	+85	+85	260	80	0 ± 30	0 ± ½
19	60	575	750	965	-2	-32	+85	+85	260	80	0 ± 30	0 ± ½
20	60	575	750	965	-2	-35	+85	+85	260	80	0 ± 30	0 ± ½
21	60	575	750	965	-2	-33	+85	+85	260	80	0 ± 30	0 ± ½
22	60	575	750	965	-2	-32	+85	+85	260	80	0 ± 30	0 ± ½
23-25	60	575	750	965	-2	-29	+85	+85	260	80	0 ± 30	0 ± ½
26	60	578	750	965	-2	-25	+85	+85	260	80	0 ± 30	0 ± ½
27	60	572	750	965	-2	-25	+85	+85	260	80	0 ± 30	0 ± ½

Geometric Scale Factor: 25.4 mm = 1 mm
Voltage Scale Factor: 1 mm = 235.3V

Table II (Concluded)

No.	L_0	L_1	L_2	L_3	G_0	G_1	G_2	G_3	R_1	R_2	Launch Angle	Launch Point
28	60	584	750	965	-2	-25	+85	+85	260	80	0 ± 30	0 ± ½
29	60	584	750	965	-2	-25	+85	+85	260	80	0 ± 10 ± 20 ± 30	0 ± ½
30	60	586	750	965	-2	-29	+85	+85	260	80	0 ± 10 ± 20 ± 30	0
Change to 3/8 inch diameter balls.												
31	60	586	750	965	-2	-29	+85	+85	260	80	0 ± 10 ± 20 ± 30	0
32	60	586	750	965	-2	-29	+85	+85	260	80	0 ± 30	0 ± ½
33	60	584	750	965	-2	0	+85	+85	260	80	0	0 ± ½
34	Velocity measurement with strobe (20 kV target = 650V launch)											
35	60	584	750	965	-2	0	+85	+85	260	80	0 ± 30	0 ± ½
36	Velocity measurement and change (20 kV target = 390V launch)											
37	60	584	750	965	-1.6	-25	+85	+85	260	80	0 ± 30	0 ± ½
38	60	710	840	965	-1.6	-24	+85	+85	260	80	0 ± 30	0 ± ½
39	60	740	840	965	-1.6	-13	+85	+85	260	80	0 ± 30	0 ± ½
40	60	740	840	965	-1.6	0	+85	+85	210	80	0 ± 10	0 ± ½
41	60	740	840	965	-1.6	0	+85	+85	260	80	0 ± 30	0 ± ½
42	60	740	840	965	-1.6	0	+85	+85	260	80	0 ± 20	0 ± ½
43	60	740	840	965	-1.6	0	+85	+85	260	80	0 ± 10	0 ± ½
44	60	790	890	965	-1.6	-8	+85	+85	215	80	0 ± 30	0 ± ½
45	60	790	890	965	-1.6	-13	+85	+85	215	80	0 ± 20	0 ± ½
46	60	790	890	965	-1.6	-16	+85	+85	215	80	0 ± 30	0 ± ½
47	60	790	890	965	-1.6	-16	+85	+85	215	80	0 ± 20	0 ± ½
48	60	790	890	965	-1.6	-16	+85	+85	215	80	0 ± 10	0 ± ½
49	60	790	890	965	-1.6	-8	+85	+85	215	80	0 ± 30	0 ± ½
50	60	790	890	1065	-1.6	-8	+85	+85	215	80	0 ± 30	0 ± ½
51	60	790	890	1065	-1.6	-8	+85	+85	215	80	0 ± 10	0 ± ½
52	60	790	890	1065	-1.6	-8	+85	+85	215	80	0 ± 10 ± 20 ± 30	0 ± ½
53	60	790	890	1065	-1.6	-8	+85	+85	215	80	0 ± 10 ± 20 ± 30	0 ± ½

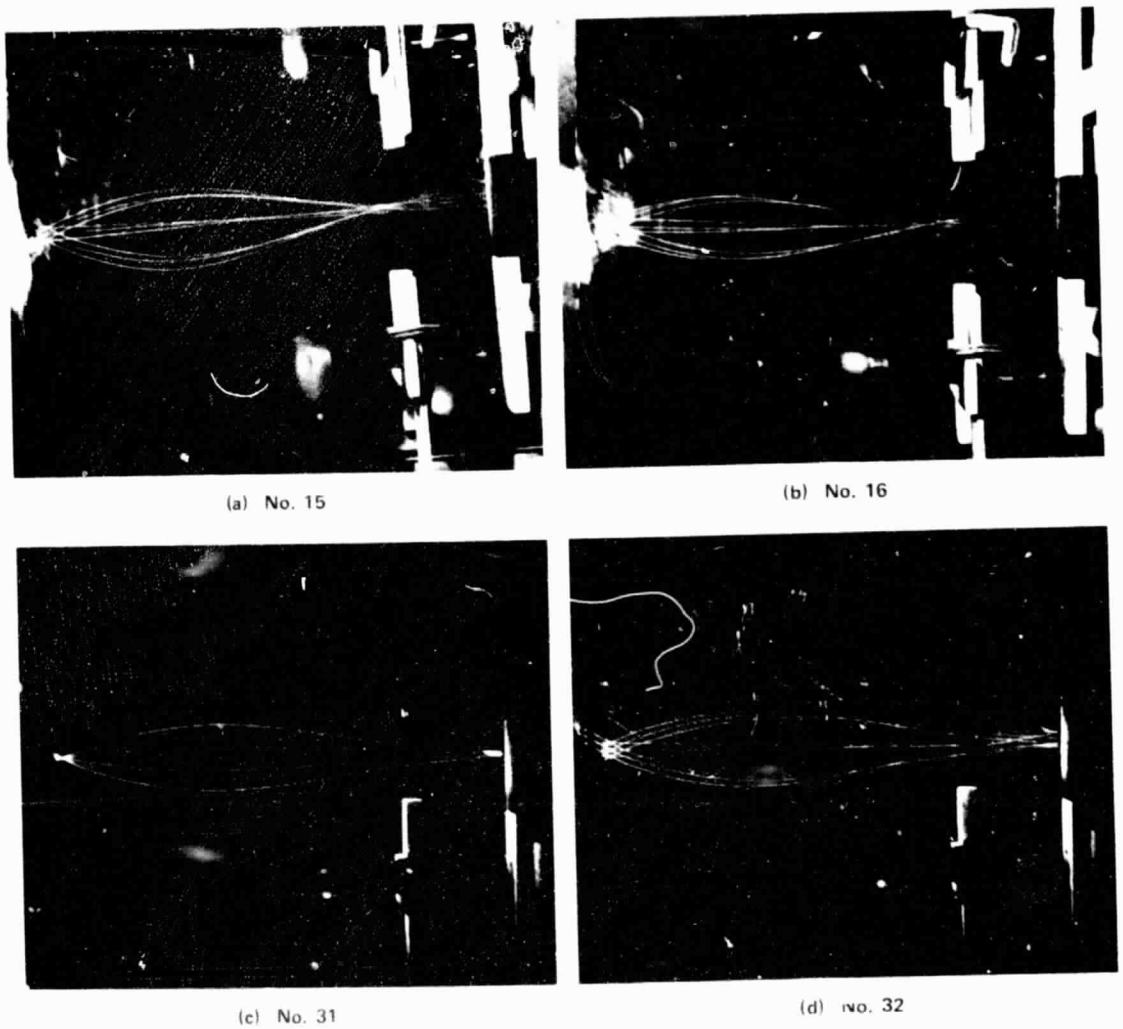

(a) No. 15

(b) No. 16

(c) No. 31

(d) No. 32

FIGURE 26 ELECTRON TRAJECTORIES MODELED ON A RUBBER-MEMBRANE TABLE; (a) AND (b) SHOW THE EFFECTS OF 5 PERCENT ELEVATION CHANGES AND (c) AND (d) SHOW THE DIFFERENCE BETWEEN ON-AXIS AND OFF-AXIS EMISSION

height and table level was very high. In Figure 26(a) the left half of electrode G_1 was 5% higher than the right half; in 26(b) the two halves are essentially the same height. The difference is seen most easily in the zero-degree-launch trajectories which in effect reversed themselves quite noticeably; the table frame was probably not exactly flat. This yields a tolerance reference for review of subsequent results.

Figures 26(c) and 26(d) (No. 31 and 32 in Table II) show trajectories with an image-forming system, i.e., with the target in the image plane. The effects of 0°, 10°, 20°, and 30° angular spreads on on-axis emission are shown in 26(c). A combined 30° angular spread and off-axis emission are shown in Figure 26(d). The 30° angle of emission is expected to be the worst case.

Figures 27(a) and 27(b) (No. 47 and 46 on Table II) are a crossover forming system, i.e., the target is in the crossover plane of the system. The effect of emission angle on beam size for 20° and 30° emission angles respectively including off-axis emission sites is shown. The off-axis sites represent the scaled extremities of the state-of-the-art 5000-tip TFFEC ($\pm$ 1/2 mm from the axis of the system).

The best overall performance is produced by the image-forming system shown in Figures 27(c) (No. 49 on Table II) and 27(d) (No. 53 on Table II). In Figure 27(d) electrode G_3 has been moved back to show the "beam" minimum without the clutter of the balls bounding off this electrode. Figure 27(d) also shows seven launches from each of the three launch sites rather than the usual three from each. These are 0°, $\pm$ 10°, $\pm$ 20°, and $\pm$ 30° from the center of the array as well as the extreme left and right edges of the scaled cathode surface. Scaling values from Table II give the following values for electrode geometry and voltage (Figure 25):

$$L_0 = 2.4 \text{ mm}, \; L_1 = 31.1 \text{ mm}, \; L_2 = 35 \text{ mm}, \; L_3 = 38 \text{ mm}$$
$$R_1 = 8.5 \text{ mm}, \; R_2 = 3.2 \text{ mm}$$
$$G_0 = 350 \text{ V}, \; G_1 = 1880 \text{ V}, \; G_2 = 20 \text{ kV}, \; G_3 = 20 \text{ kV}.$$

These values were used as a starting point in setting up an electron optics bench experiment for electron gun tests.

3. Computer Model of the Immediate Vicinity of the Cathode Tip

Although the rubber table was helpful in investigating electron gun geometry, modeling the individual tip region accurately would be very difficult with this technique. To help investigate this region and to obtain data on the emission angles that might be expected from the tips, a computer program was used that had been developed for a previous study at SRI to ascertain the equipotentials in the cathode gate-tip region.

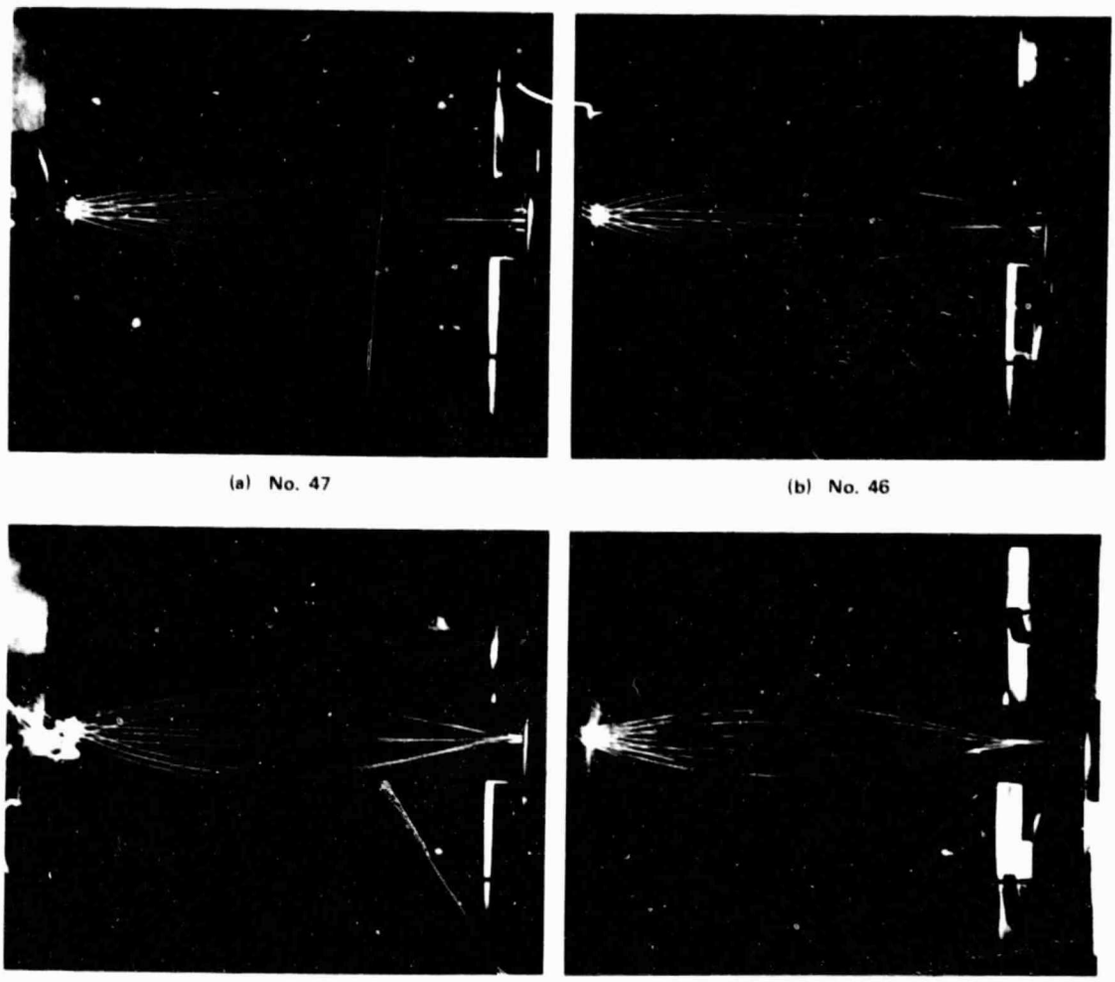

(a) No. 47 (b) No. 46

(c) No. 49 (d) No. 53

FIGURE 27 ELECTRON TRAJECTORIES MODELED ON A RUBBER MEMBRANE TABLE; (a) AND (b) SHOW A CROSSOVER-FORMING SYSTEM FOR 20° AND 30° MAXIMUM LAUNCH ANGLES RESPECTIVELY, AND (c) AND (d) SHOW AN IMAGE-FORMING SYSTEM

A representative set of cathode dimensions was chosen for the computation as follows: gate electrode thickness 0.4 μm; diameter of the hole in the gate electrode 1.3 μm; silicon dioxide thickness 1.4 μm; cone height 1.4 μm; cone base diameter 1.0 μm; tip radius 0.05 μm. The computation of the electric field around the tip was made using a Control Data Corporation 6400 digital computer and using the relaxation methods to solve LaPlace's equation in the interelectrode region. By using successively smaller mesh sizes, the equipotentials could be obtained to any degree of accuracy. Figure 28 shows the calculated relative field conversion factor (β) for this geometry as a function of the polar angle (θ), measured from the center of curvature of the tip. It is seen that the field is essentially constant to 30° and then begins to fall off slowly. If we were dealing with a perfectly smooth tip we would expect to see constant current density up to an angle of 30°, and significant current at angles approaching 60°; but as discussed earlier the tip is not ideally smooth and in practice we seem to be dealing with local field enhancement resulting from surface conditions not accounted for in the computer model. Nevertheless, it is clear from this computation that large-angle emission is possible with this kind of structure.

4. Electron Optics Bench

An electron optics bench was fabricated for testing the cathode gun geometry. The original system (Figure 29 and 30) consisted of a fixed cathode mount (K), shields (19 & 34), a movable focusing lens (12), a fixed accelerating electrode (13), a movable phosphor (14). The focus electrode (12) and phosphor (14) were adjustable while operating the gun: it was possible to study a variety of lens locations and measure beam profiles by moving the phosphor along the z axis of the gun while making spot diameter measurements.

The electron-optics bench was mounted in an ion pumped system and pumped $\sim 5 \times 10^{-9}$ torr with mild ($\sim$ 100°C) bakeout. The cathode was then turned on with the tips driven negative and the gate grounded. Electrode voltages were increased slowly while monitoring system pressure and cathode current. The emission was usually stabilized at between 5 and 20 μA with the target at 20 kV.

The phosphor originally used was a transparent coating of willemite on a Vycor substrate that was coated with tin oxide for conductivity. The phosphor was obtained from Liberty Mirror, a division of Libbey-Owens-Ford Company; this phosphor was chosen because it is smooth and is processed at high temperatures ($\sim$ 1000°C) and therefore relatively clean. It worked well and was very bright at low current levels, although as we probed into the "higher" current realm, e.g., over 20 μA at 20 kV, and spot sizes of less than 1 mm, the phosphor was damaged. Subsequent work was done with a thin film rare earth oxide ($Y_2O_3 + Tb_4O_7$) phosphor. This phosphor was fabricated in the laboratory by physical vapor deposition onto a sapphire substrate using electron

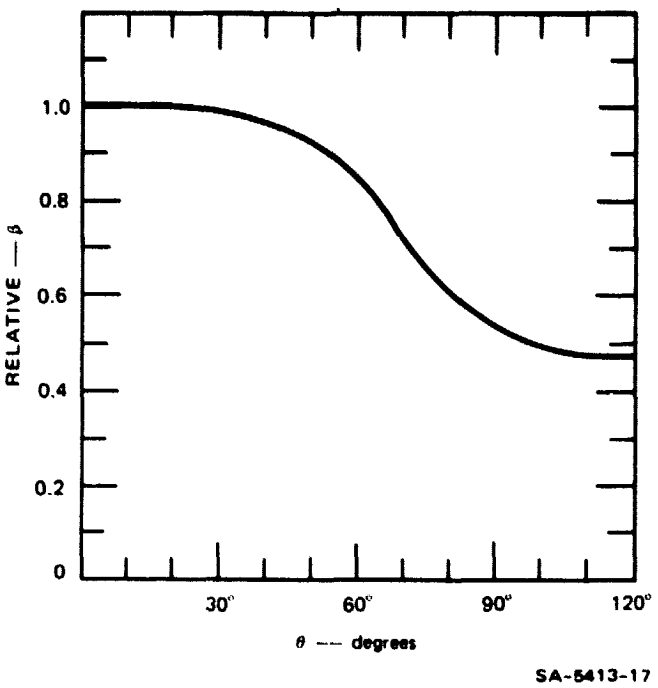

FIGURE 28 COMPUTED RELATIVE FIELD-CONVERSION FACTOR AS A FUNCTION OF THE POLAR ANGLE θ MEASURED FROM THE CENTER OF CURVATURE OF THE TIP

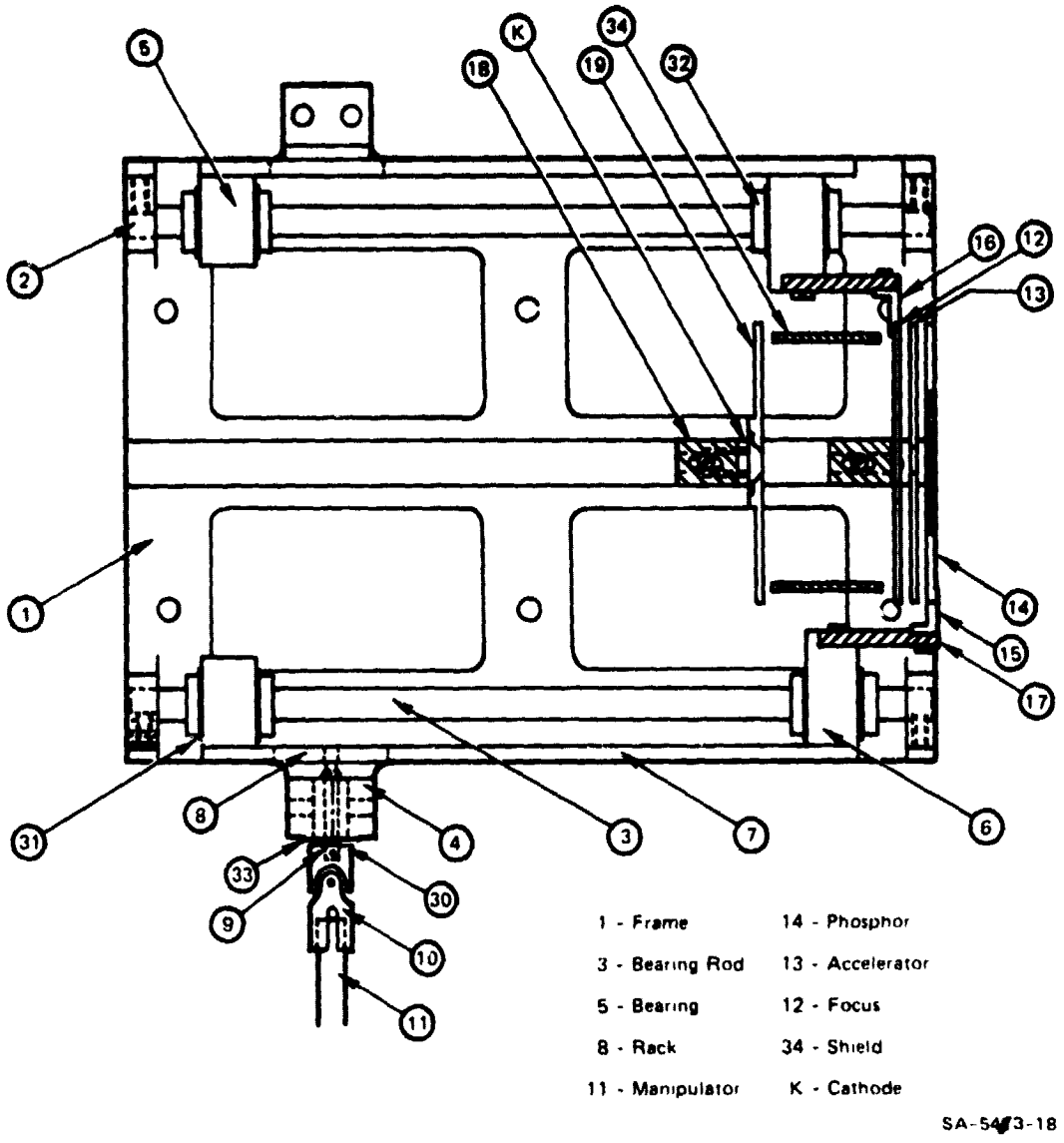

FIGURE 29 PLAN VIEW OF THE ELECTRON-OPTICS BENCH WITH KEY COMPONENTS IDENTIFIED

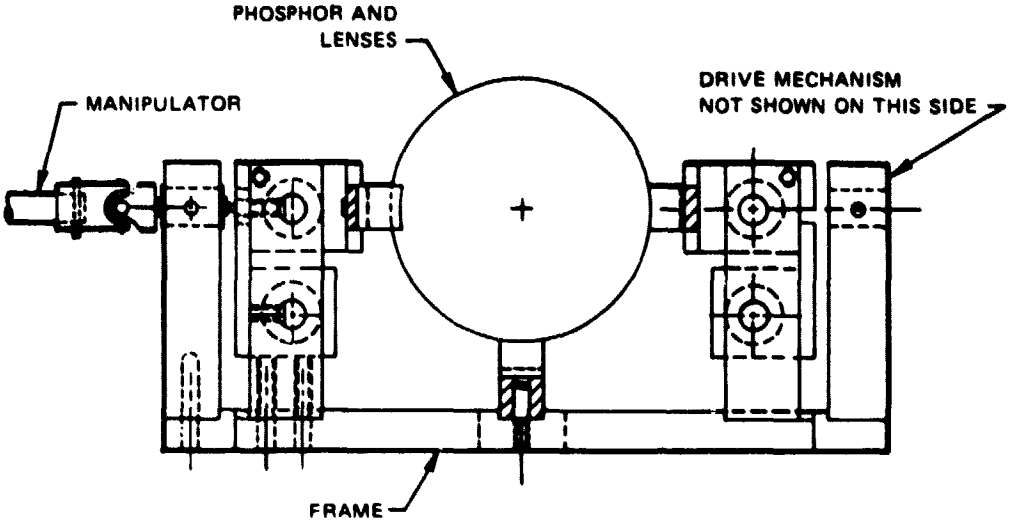

FIGURE 30 FRONTAL ELEVATION OF THE ELECTRON OPTICS BENCH

beam evaporation. The phosphor was coated with aluminum for conductivity and found to work very well in this application.

The geometric setup for the first test is shown schematically in Figure 31. The cathode was mounted on a TO-5 header, (a standard commercial 8-pin transistor header, Haledon Industries), and a shield (S_1) was mounted on the header to shield electrostatic field asymmetries caused by the mounting structure and gate film contact. All shields, S_1, S_2, and S_3 were electrically insulated and connected to feedthroughs so that the potential on the shields could be changed and the effect on beam properties observed. From these observations, changes in shield electrode geometries could be made to obtain optimum performance with the shield at some common potential such as ground or cathode potential. V_5 was set at 20 kV while V_4 was varied and beam diameters measured for various positions of G_1 and the phosphor (G_3). The phosphor was electrically connected to the accelerating electrode (G_2) but mechanically free to be moved relative to G_2.

Beam diameter measurements were made on the phosphor using a traveling telescope. The measurements were made at the full diameter of the visible spot rather than the half height of the beam current profile as is the practice in display work. The minimum spot size obtained was in the range of 0.25 mm with this gun arrangement. Figure 32 summarizes the results.

The first measurements were made with the shields grounded, V_5 at 20 kV, and the focus voltage varied as shown in Curve 1, Figure 32. With this configuration we observed indications of electron scattering off either the gate film or S_1 or both in the form of radial rays emanating from a well-defined spot.

Experimentation with the voltages on the shields reduced the rays to a level that was not visible on the phosphor. Curve 2, Figure 32, shows the spot size as a function of focus voltage for this electrical configuration. It is interesting to note that with the voltages shown for Curve 2, a slightly magnified image of the cathode array was visible on the phosphor when the focus voltage (V4) was zero. The minimum spot size obtained with this configuration was about 0.3 mm, but the spot was much more clearly defined that it had been with the shields grounded, and the radial rays were no longer prominent.

These results suggested that the angular spread could be minimized by placing a positive electrode in the system as shown in Figure 33. Here shield S_3 has been removed; an electrode (G_4) has been added to help accelerate the electrons and turn them toward the axis by lens action in combination with shield S_1. Figure 34 shows the beam diameter as a function of focus voltage (V_4) for this configuration. Many combinations of V_1, V_3, and V_4 were found to produce essentially the same result (again the tip array was imaged at $V_4 = 0$). The beam current during these measurements was varied between 5 μA and 10 μA. Higher currents made measurements difficult because of the extreme brightness of the phosphor.

	ID	WIDTH	DISTANCE FROM THE CATHODE
S_1	4.5 mm	0.13 mm	0.5 mm
S_2	10 mm	0.13 mm	0.5 mm
S_3	40 mm	20 mm	2 mm
G_1	17.4 mm	1.2 mm	VARIABLE
G_2	6.8 mm	1.2 mm	33.3 mm

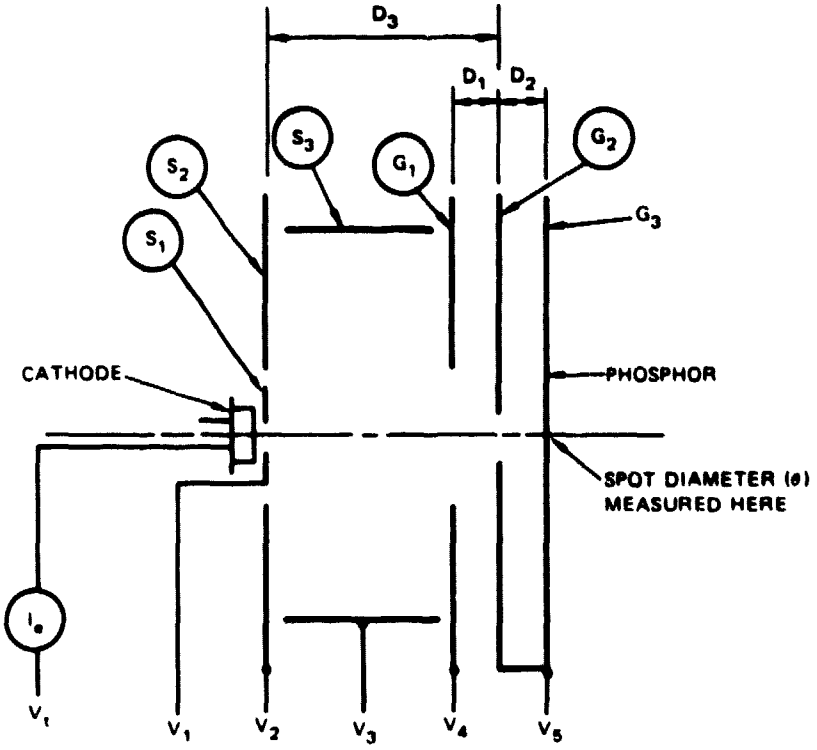

FIGURE 31 TEST BENCH CONFIGURATION FOR FIRST SPOT-SIZE MEASUREMENTS

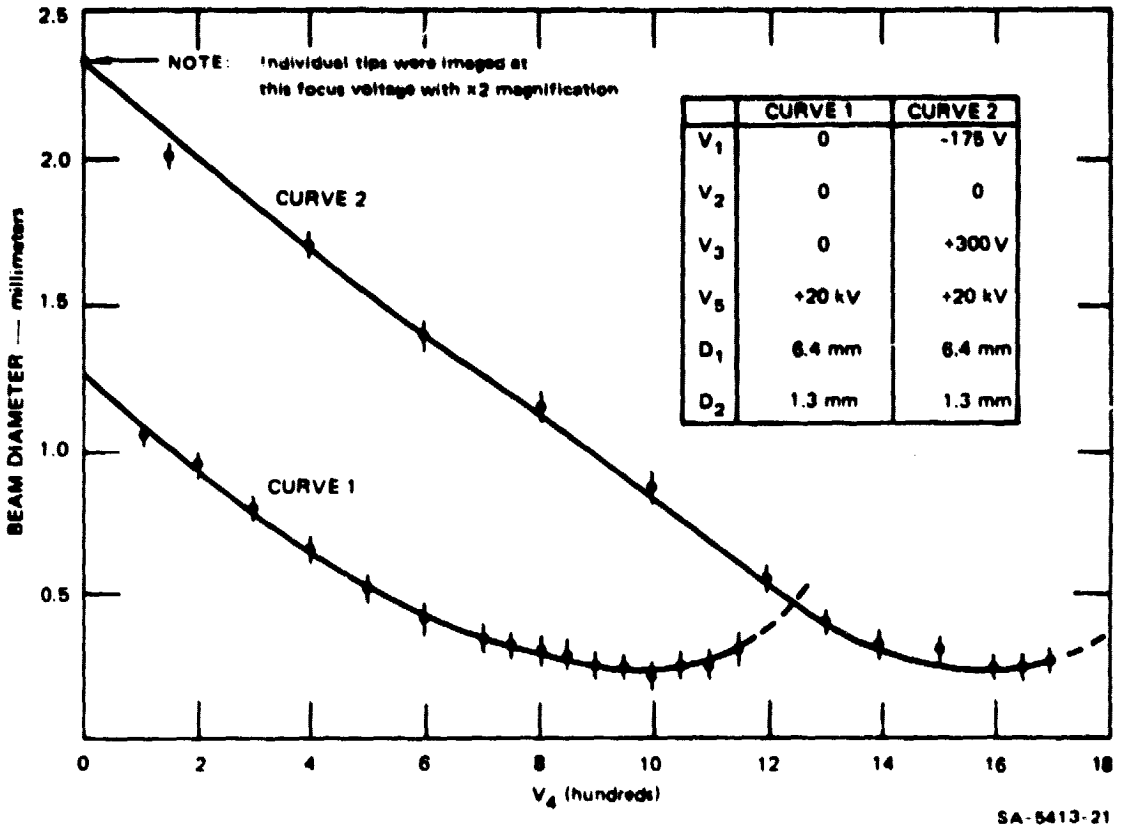

	CURVE 1	CURVE 2
V_1	0	-175 V
V_2	0	0
V_3	0	+300 V
V_5	+20 kV	+20 kV
D_1	6.4 mm	6.4 mm
D_2	1.3 mm	1.3 mm

FIGURE 32 SPOT SIZE AS A FUNCTION OF FOCUS VOLTAGE WITH THE ELECTRODE GEOMETRY SHOWN IN FIGURE 31

	ID	WIDTH	DISTANCE FROM CATHODE
S_1	4.5 mm	0.13 mm	0.5 mm
S_2	10 mm	0.13 mm	0.5 mm
G_1	17.4 mm	1.2 mm	VARIABLE
G_2	6.8 mm	1.2 mm	33.3 mm
G_3	—	—	VARIABLE
G_4	4.8 mm	1.2 mm	6 mm

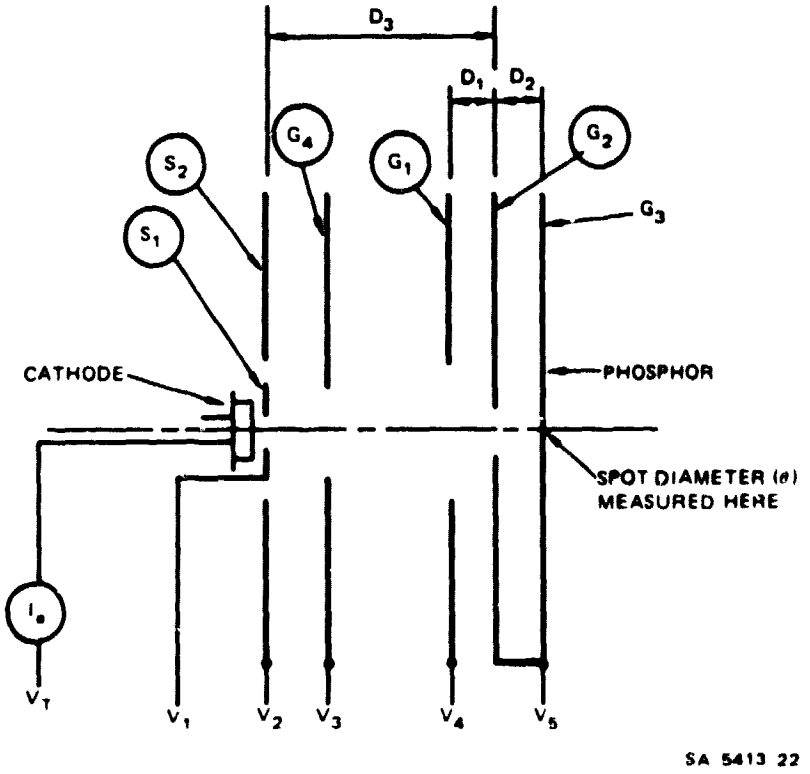

FIGURE 33 SECOND GUN CONFIGURATION FOR TEST BENCH MEASUREMENTS OF BEAM DIAMETER

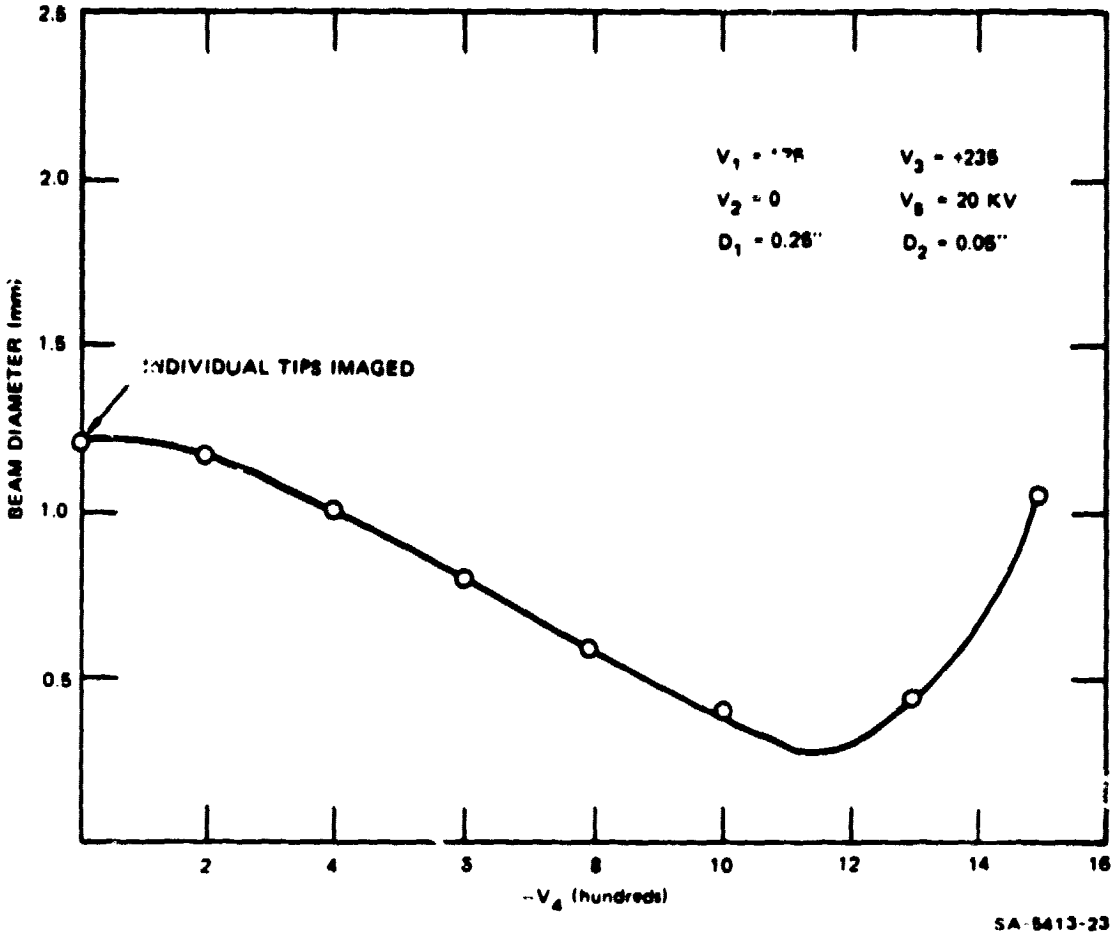

FIGURE 34 BEAM DIAMETER FOR VARIOUS FOCUS VOLTAGES
Second gun configuration.

Figure 35 shows the beam profile along the z-axis of the system. The phosphor was moved along the z-axis and measurements of beam diameter made while keeping everything else in the system constant. It can be seen that the angles are much like those seen with the rubber-membrane model (Figure 26(d)). The radial rays seen with the first configuration were not seen here at 20 μA. Careful observation of the cathodes used indicated that most of the ray effect originated at fault sites on the cathode; i.e., spurious emissions from a damaged emitter site.

Although these results are very encouraging, it is clear from concurrent high emission tests that when operating at the currents required by NASA (~ 95 mA) the effects of space charge can produce difficulties. These problems are in the form of excessive gate film bombardment and beam spreading unless the fields at the cathode surface are sufficiently high to prevent space charge. In additon, trajectory plots obtained from the NASA Lewis program indicated that at 100 mA the beam diverged in the immediate vicinity of the cathode with the gun configuration shown in Figure 31 and rays emitted at high angles could strike the lens elements.

The configuration shown in Figure 33 can overcome this difficulty by applying a large voltage to V_3. NASA-Lewis ran a trajectory plot of a similar gun configuration that they designed to eliminate this difficulty. Figure 35 shows the NASA gun configuration and the computed electron trajectories for $V_3 = V_5 = 20$ kV and $V_4 = 0$. These trajectories show that low angle emission will be fairly well behaved at 100 mA beam currents, but according to this model emission at angles of 30° will not traverse the gun structure.

The gun geometry shown in Figure 36 was set up on the electron-optics bench and spot-size measurements were made. The gun worked well with a minimum spot size of ~ 0.25 mm measured when G_1 was -600 V and $G_2 = G_4 = 20$ kV. Current used for the measurement was 10 μA. Tests must be made on a tube structure or NASA's beam tester to determine whether or not the emission angle becomes large enough to cause difficulty when the current reaches the 100 mA level.

1. Precision Cathode Mount

It is necessary that the assembly be done as neatly as possible if the gun is to perform to its maximum capabilities. Tolerances on crucial parts are held at + 0.0005 inch and the cathode must be positioned to comparable tolerances if the design is to meet expectations. The cathode mount must also meet several other requirements for the present program. These can be summarized as follows:

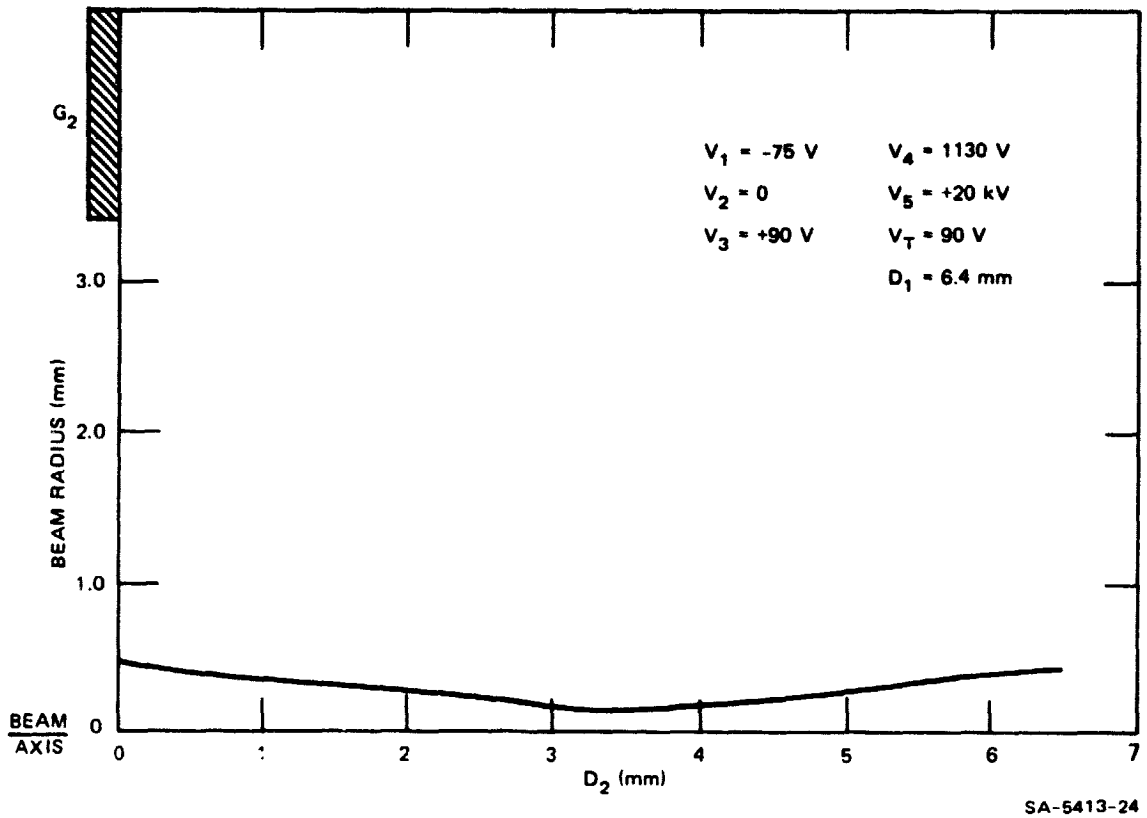

FIGURE 35 EXAMPLE OF THE BEAM ENVELOPE

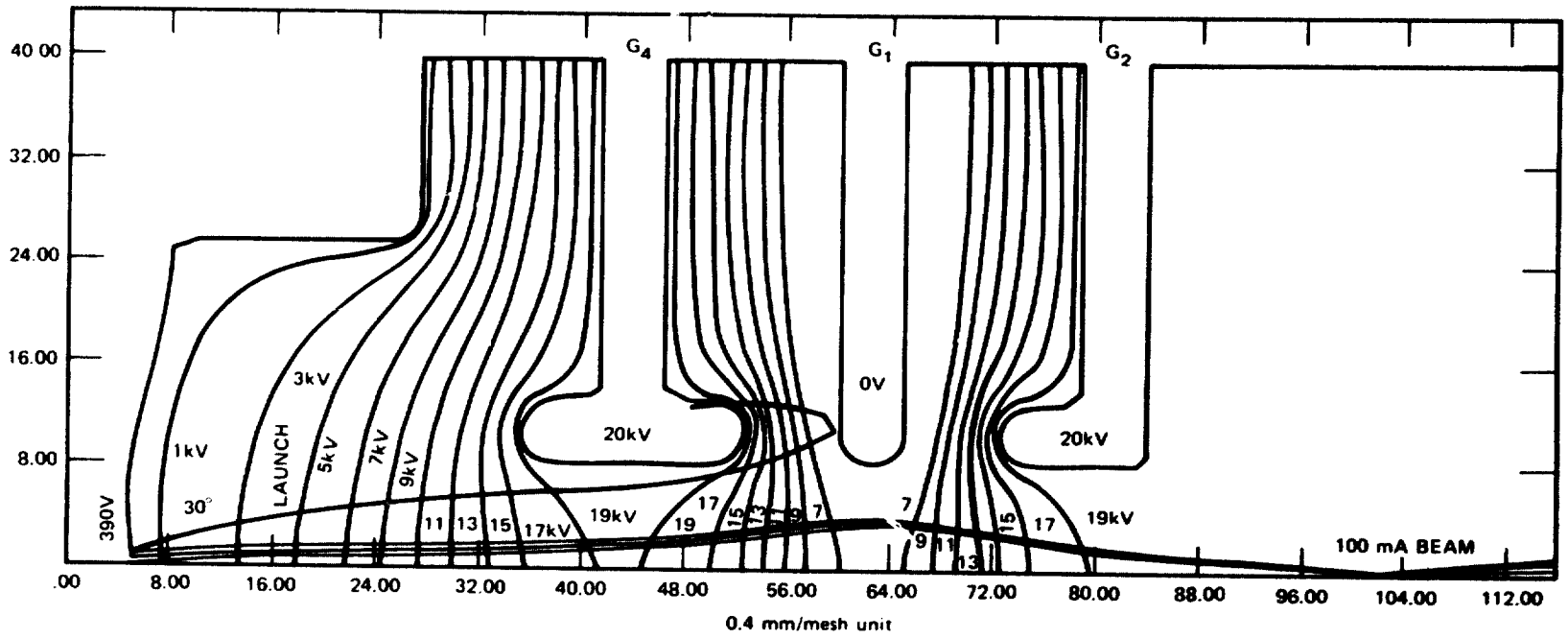

SA-5413-25

FIGURE 36 THIRD GUN CONFIGURATION USING NASA GEOMETRY AND SHOWING COMPUTER-PLOTTED TRAJECTORIES FOR 100 mA BEAM

(1) The mount must be bakeable to at least 450°C.

(2) The cathode must be easily replaceable in the mount.

(3) The cathode must be aligned to within 0.001 inch of the axis of the mount.

(4) The mount must be self aligning with the rest of the gun structure within 0.001 inch.

(5) The mount assembly must be shock resistent and rugged enough to ship across the country without loss of alignment.

(6) The mount must be compatible with, or must incorporate in its own shape the required electrode shapes for the gun design.

A joint NASA/SRI staff effort produced the design shown in Figure 37. The cathode chip is clamped in position between the mount/ focus electrode structure and a molybdenum spring. The spring is made in two pieces as shown to accommodate thermal expansion effects, and is a low mass part so there is no danger of shock loads cracking the silicon cathode chip.

The 1-mm diameter emitter tip array is not centered on the chip, and the chip has irregular dimensions that cannot be used for reference because it is scribed and broken out of a larger silicon substrate. Thus, it is necessary to align each cathode with the focus electrode visually using a microscope, simple manipulator, and jig built for the purpose. The procedure is done basically by hand and requires some operator skill, however, it works well and elaborate manipulators would be very expensive by comparison. Figure 38 is a photograph of the mount with a cathode in place. The front view shows the Pierce-like geometry of the focus electrode that is an integral part of the mount. The gate film is in physical and electrical contact with the focus electrode. The mount surface is gold coated to improve contact and prevent scratching. A wire spot-welded to the molybdenum hold-down spring is the electrical lead for contact to the base or emitter-tip array.

J. Electron Gun Delivered to NASA

While the electrode configurations described in Section H above show promise in production of the desired beam configuration, NASA must, as a practical matter, be concerned with maintaining the minimum number of electrodes in the tube structure. With this goal, a design was developed at NASA with the aid of the NASA computer program. Figure 39 shows a computer simulation of the gun. This design was used to fabricate a gun by a commercial tube manufacturer (Watkins-Johnson Company) using standard tube-fabrication technology. Figure 40 shows the gun layout (detailed engineering drawings of the gun structure were delivered to NASA with the gun assembly). The design features the demountable cathode-mount assembly

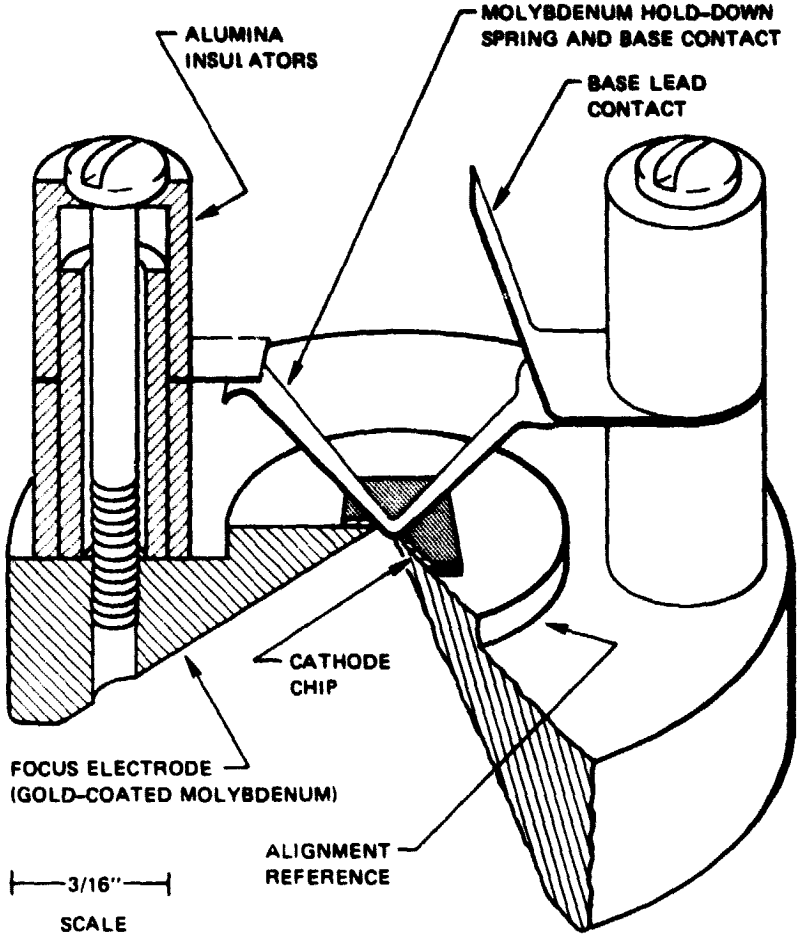

FIGURE 37 ISOMETRIC DRAWING OF CATHODE MOUNT AND FOCUS ELECTRODE

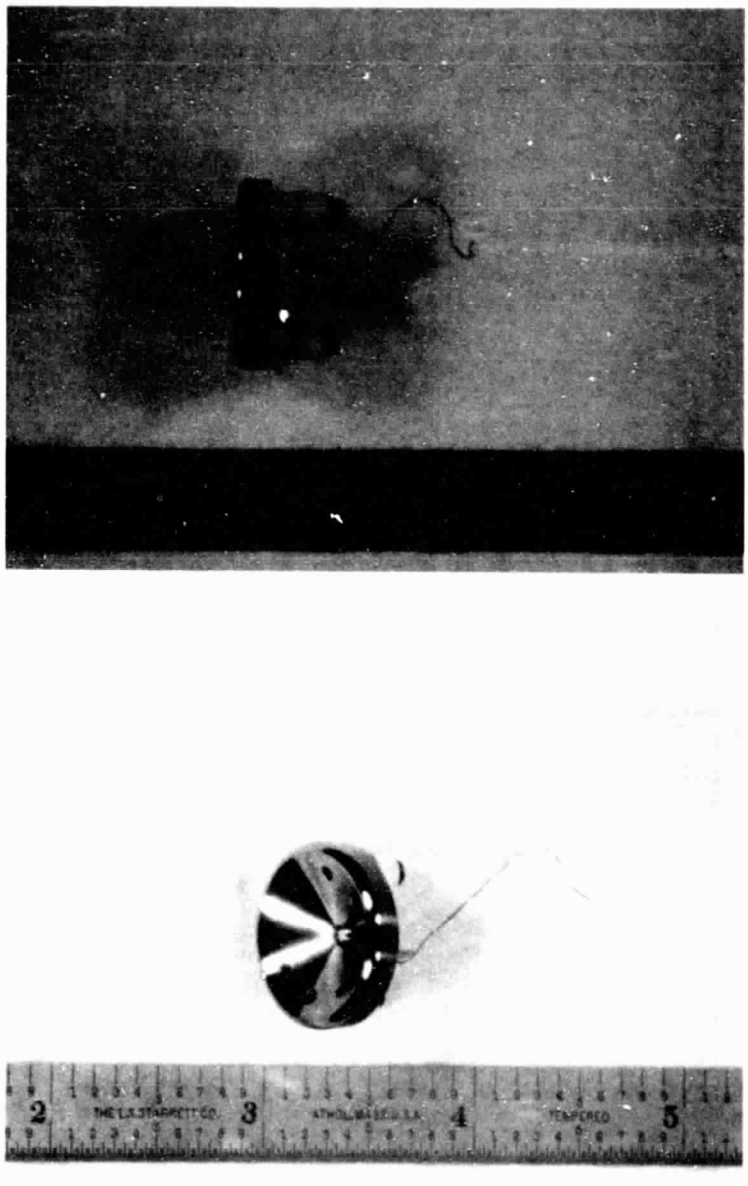

FIGURE 38 SIDE VIEW AND FRONT VIEW OF CATHODE MOUNT WITH A CATHODE IN PLACE

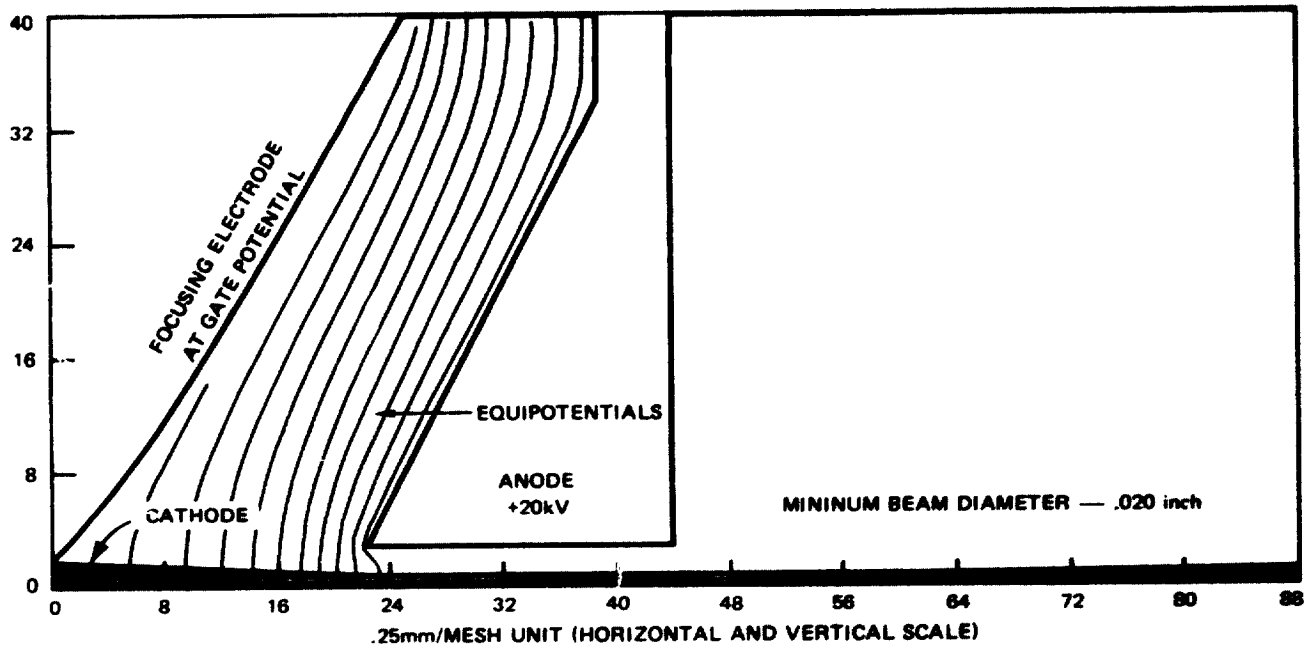

FIGURE 39 COMPUTER PLOTTED TRAJECTORIES FOR TWO-ELECTRODE GUN

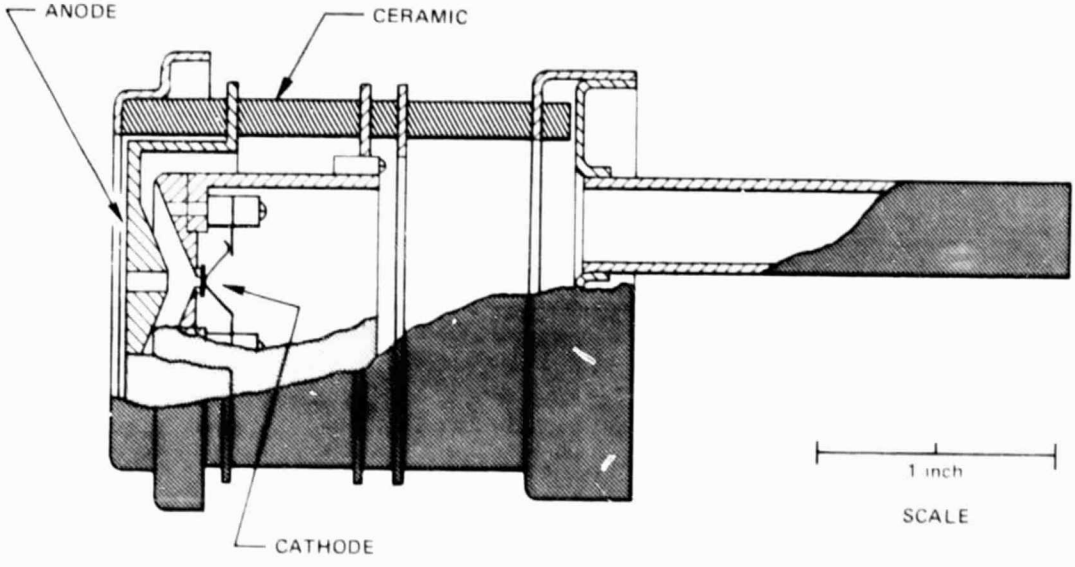

FIGURE 40 NASA/WATKINS-JOHNSON ELECTRON GUN DESIGN

(described in the preceding section) that allows the cathode to be replaced and to be precisely aligned in the gun structure.

Two guns were fabricated by Watkins-Johnson and delivered to SRI. A cathode was installed in the first gun, and the entire gun structure was mounted in a 4-inch ID appendage to an ion pumped vacuum system. The appendage was wrapped with heating tape and baked to ~ 300°C when under vacuum for outgassing.

A phosphor target was included in the first test set-up so that the beam shape could be observed as a function of the applied focus voltage. However, we were not able to take advantage of the phosphor as a result of electrical feedthrough and power supply limitations. The gun was designed to operate with a 12 kV accelerating focus voltage, but we were only able to use 1.2 kV with this setup. Thus, observations of the focus were not possible. In addition, the emission during the experiment was limited to about 1 mA as higher currents were damaging to the phosphor. Nevertheless, the cathode behaved well during the first gun test. Emission was brought up to 1 mA and held at that level for 25 hours without difficulty. The gun was then removed from the vacuum system and shipped to NASA.

Figure 41 shows a cathode mounted in gun number two and the voltage-current curve obtained when this cathode was tested in the gun. This cathode had been previously operated at 80 mA in our high current tests. (Only two tips were blown during these tests--the other flaws are due to photography and printing.) The relatively high gate current shown was due to the mounting structure, and is not a property of this cathode (this fault was essentially eliminated in later tests). In all gun tests at SRI the voltage on the anode was limited to 1.2 kV instead of the design value of 12 kV. NASA computer simulations showed that under these conditions the emission current should be limited to 10 mA, since the effects of space charge at higher current levels cause some electrons to return to the gate film rather than traverse the gun structure (see Figure 6).

Additional cathodes were mounted in the second gun at SRI and tested. The results are summarized in Table III. The results with cathodes 20-44-2-H and 20-45-2-P are surprising. The first had been baked and run at 330°C in the initial test and had performed well at 90 mA. Examination after this test showed that 44 tips had blown. Cathode 20-45-2-P was baked and tested at 400°C and taken to 50 mA. Subsequent examination showed that none of the 5000 tips had failed. This suggested that 400°C was helpful in cleaning up the environment and cathode to eliminate failures caused by discharges, but neither cathode performed well in the gun structure when baked and operated at 400°C. It appears that 400°C on the gun structure created a very poor local vacuum environment, or that some form of contamination entered the gun structure. This has apparently been remedied as a subsequent experiment was successful using a 400°C bake for cleaning, and a cool down to 270°C prior to emission tests.

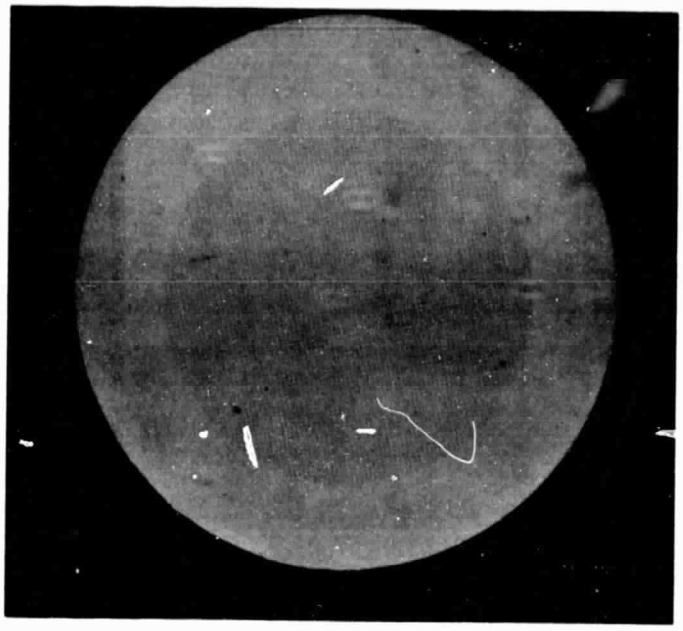

(a) CATHODE 20-42-2-P CENTERED IN THE CATHODE MOUNT

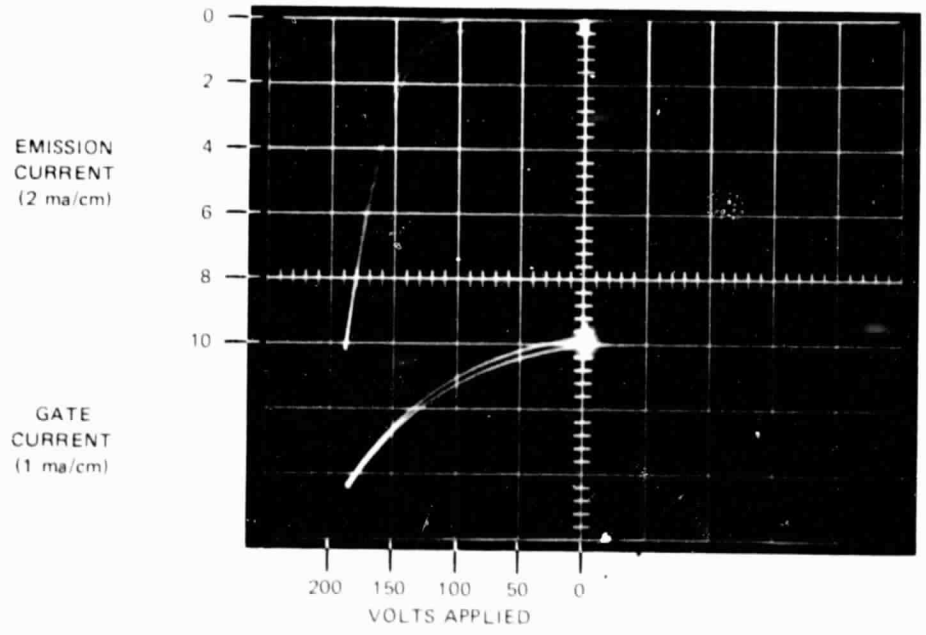

(b) EMISSION IN NASA GUN

FIGURE 41 CATHODE 20-42-2-P IN THE NASA ELECTRON GUN STRUCTURE

Table III

RESULTS OF TESTS IN THE NASA GUN STRUCTURE

Cathode	Initial Test at ~ 350°C	Gun Test	Temperature Bake	Temperature Test	Remarks
20-1i-1-P	110 V/10 mA	155 V/10 mA	300°C	300°C	Blown by a high voltage arc.
20-16-1-R	225 V/95 mA	170 V/1 mA	300°C	300°C	Shipped to NASA in gun #1. OK
20-42-2-P	210 V/80 mA	185 V/10 mA	300°C	300°C	Shipped to NASA. OK
20-9-1-L	180 V/105 mA	220 V/.5 mA	300°C	300°C	Damaged by voltage accident
20-11-1-F	150 V/50 mA	165 V/5 mA	330°C	330°C	Shipped to NASA. OK
20-44-2-D	205 V/80 mA	215 V/5 mA	300°C	300°C	Shipped to NASA. OK
20-44-2-H	250 V/90 mA	155 V/3 mA	400°C	400°C	Shorted. ~ 1000 tips blown
20-45-2-P	130 V/50 mA*	130 V/4 mA	400°C	400°C	Shorted. ~ 1000 tips blown
20-45-2-O	105 V/35 mA*	130 V/3 mA	400°C	400°C	Shipped to NASA. OK

*400°C in initial test

III SUMMARY

The goal of this program was the delivery to NASA of a prototype electron gun with a field emitter array cathode capable of 95 mA emission; the gun was to produce a beam 1/4 mm in diameter at 12 kV. Achievement of this goal required supporting studies in the areas of cathode fabrication, cathode performance, gun design, cathode mounting, and gun fabrication.

A series of empirical investigations advanced the fabrication technology: a study which used an ion-pumped vacuum system for film deposition and cone formation and a study of the effects of deposition and etching parameters on the geometry of the final structure were particularly important. Deposition of the cones in a clean ion-pumped vacuum system should produce a cleaner tip and therefore a more stable emitter. Improved adhesion between the molybdenum gate film and the silicon dioxide insulating layer has definitely improved the geometry of the structure through reducing the undercutting of the gate film during the oxide etch. This improvement nearly eliminated failures due to cracking of the gate film, reduced the incidence of multiple cone failures caused by chain reaction discharges, and opened the way for development of a cathode which has packing densities higher than the present 6400 mm^{-2}.

The cathode performance studies indicate that the cathode is capable of producing well over 95 mA with ease; but anode, or collector, configurations and driving circuits become important factors when operating at the power levels involved. A substantial collector development effort was required to show that the cathode is indeed capable of emission levels in the 100 mA region.

The collector development could be carried further in order to investigate maximum currents, but it was shown that a simple stainless steel tube mounted with its axis on center with the cathode was capable of handling pulsed 100-mA currents with about 1-kV energies, although space charge problems made these levels difficult to achieve. In one case, 160 mA was demonstrated. This is 20 A/cm^2 from the cathode and well in excess of the program goal.

Life tests initiated during the previous program have demonstrated that a 100-tip cathode can maintain 2-mA peak 60-Hz emission for more than 33,000 hours of operation. This is an average emission of 20 μA per tip which is the emission required to give 100 mA (12 A/cm^2) from a 5000-tip array of the kind used in this program. Thus, it is reasonable to expect that long life can be obtained with the 5000-tip array operating at 100 mA with a well designed collector.

Most failures apparently occur early in testing; there seems to be potentially damaging pressure bursts from the cathode and anode structures as the emission is increased. Once emission has been established at a given level, however, the cathode is capable of withstanding rather ordinary pressure environments (up to 10^{-5} torr). These pressure bursts are likely to be the cause of our difficulty with cathodes 20-44-2-H and 20-45-2-P (Table III). Both cathodes performed very well in the initial tests, but blew large numbers of tips when tested in the NASA/Watkins-Johnson gun structure: the failures were like those we saw with the copper collector experiment (Table I). We conclude that anode processing is crucial, and that a specific process and materials investigation should be carried out to settle this question.

The multiple-peak results obtained in the energy spread experiments were not expected, and have not been adequately explained. Reason suggests that the cause of the multiple peaks in the energy-distribution curves was an artifact of the electron optics of the experimental setup, as the system was meant to be used with a single on-axis source. The developer of the system (van Oostrom) did similar experiments and obtained the same results, therefore it was assumed that the result was not due to our particular setup, but the general approach. The complexity of any alternate approach precluded further efforts to measure energy spread on this program.

Electron gun designs were modeled on a rubber-membrane table and with a NASA computer program. Configurations that showed promise were set up on an electron optics bench in a demountable ultravacuum system and beam shapes were studied by using a manipulatable phosphor as the target and measuring beam spot diameters. These tests showed that the gun designs were capable of producing the required 20-kV 0.26-mm diameter beam when operating at low currents ($\leq$ 20 μA). Higher currents were not possible because of the limited power handling capability of the phosphor target.

High current tests in a diode configuration (i.e., with the stainless steel tube collector) showed that at high currents space charge in the immediate vicinity of the cathode could cause some electrons to return to the gate film and produce excessive heating because of bombardment of the gate. It is clear that the same effect could result in excessive spreading of the beam in and difficulty with electron gun designs that worked well at lower currents. NASA-developed computer models confirmed that beam spreading caused by space charge could cause the beam traversing the gun structure to hit the electrodes.

NASA also requires a minimum number of electrodes in the gun structure. A two-electrode gun structure was developed for this purpose using the NASA computer model. Two such gun structures were fabricated at Watkins-Johnson and delivered to SRI for cathode mounting and preliminary tests. The guns feature a demountable cathode and focus electrode structure for ease in geometry modification and cathode replacement. A simple jig was built for aligning the cathode to within 0.001 inch in the mount, and the mount is self-aligning with the gun structure to 0.001 inch.

One gun was set up and tested at SRI and then sent to NASA for evaluation in their beam tester. The second was kept at SRI and used to test cathodes prior to delivery to NASA for use in their gun. Five cathodes were pretested in our diode configuration with the stainless-steel tube collectors, mounted in the gun for tests between 3 mA and 10 mA, and then delivered to NASA for test in the beam tester.

REFERENCES

1. R.H. Fowler and L. Nordheim, "Electron Emission in Intense Electric Fields," Proc. Royal Soc. (London), Vol. A119, pp. 173-181 (1 May 1928).

2. R.B. Burgess, H. Kroemer, and J.M. Houston, "Corrected Values of Fowler-Nordheim Field Emission Functions v(y) and s(y)," Phys. Rev., Vol. 90, No. 4, p. 515 (15 May 1953).

3. W.P. Dyke and W.W. Dolan, Advances in Electronics and Electron Physics, Vol. 8, p. 98 (Academic Press, New York, New York, 1956).

4. I. Brodie, "Bombardment of Field-Emission Cathodes by Positive Ions Formed in the Interelectrode Region," Int'l. J. of Electronics, Vol. 38, No. 4, pp. 541-550 (April 1975).

5. R. Gomer, Field Emission and Field Ionization, Harvard Monographs in Applied Science, No. 9, p. 195 (Harvard University Press, Cambridge, Massachusetts, 1961).

6. C. Spindt, I. Brodie, L. Humphrey, and E.R. Westerberg, "Physical Properties to Thin-Film Field Emission Cathodes with Molybdenum Cones," J. of Appl. Phys., Vol. 47, No. 12, pp. 5248-5263 (December 1976).

7. A. van Oostrom, "Field Emission Cathodes," J. of Appl. Phys., Vol 33, No. 10, pp. 2917-2922 (October 1962).

8. R.D. Young and E.W. Müller, "Experimental Measurement of the Total-Energy Distribution of Field-Emitted Electrons," Phys. Rev., Vol. 113, No. 1, pp. 115-120 (1 January 1959).

9. A. van Oostrom, "Validity of the Fowler-Nordheim Model for Field Electron Emission," Philips Research Reports Supplement, No. 1, p. 102 (1966).

10. R. Stratton, "Energy Distributions of Field Emitted Electrons," Phys. Rev. Vol. 135, No. 3A, pp. 794-805 (3 August 1964).

11. R.W. Strayer, W. Mackie, and L.W. Swanson, "Work Function Measurements by the Field Emission Retarding Potential Method," Surface Science, Vol. 34, No. 2, pp. 22-248 (January 1973).

12. P.H.J.A. Kleynen, Philips Tech. Rev., Vol. 2, p. 321 (1937).